Drosophila models of pathogenic copy-number variant genes show global and non-neuronal defects during development

Short title: Non-neuronal defects of fly homologs of CNV genes

Tanzeen Yusuff[1,4], Matthew Jensen[1,4], Sneha Yennawar[1,4], Lucilla Pizzo[1], Siddharth Karthikeyan[1], Dagny J. Gould[1], Avik Sarker[1], Yurika Matsui[1,2], Janani Iyer[1], Zhi-Chun Lai[1,2], and Santhosh Girirajan[1,3]*

1. Department of Biochemistry and Molecular Biology, Pennsylvania State University, University Park, PA 16802
2. Department of Biology, Pennsylvania State University, University Park, PA 16802
3. Department of Anthropology, Pennsylvania State University, University Park, PA 16802

[4] contributed equally to work

*Correspondence:
Santhosh Girirajan, MBBS, PhD
205A Life Sciences Building
Pennsylvania State University
University Park, PA 16802
E-mail: sxg47@psu.edu
Phone: 814-865-0674

ABSTRACT

While rare pathogenic copy-number variants (CNVs) are associated with both neuronal and non-neuronal phenotypes, functional studies evaluating these regions have focused on the molecular basis of neuronal defects. We report a systematic functional analysis of non-neuronal defects for homologs of 59 genes within ten CNVs and 20 neurodevelopmental genes in *Drosophila*. Using wing-specific knockdown of 136 RNA interference lines, we identified qualitative and quantitative phenotypes in 72/79 homologs, including six lines with lethality and 21 lines with severe wing defects. Assessment of 66 lines for tissue-specific effects showed no correlation between the severity of wing and eye-specific defects. We observed disruptions in cell proliferation and apoptosis in larval wing discs for 23/27 homologs, and altered Wnt, Hedgehog and Notch signaling for 9/14 homologs, including *AATF/Aatf*, *PPP4C/Pp4-19C*, and *KIF11/Klp61F*. These findings were further validated with differences in human tissue-specific expression and network connectivity of CNV genes. Our findings suggest that multiple genes within each CNV differentially affect both global and tissue-specific developmental processes within conserved pathways, and that their roles are not restricted to neuronal functions.

INTRODUCTION

Rare copy-number variants (CNV), or deletions and duplications in the genome, are associated with neurodevelopmental disorders such as autism, intellectual disability (ID), and schizophrenia [1,2]. While dosage alteration of CNV regions contribute predominantly to defects in nervous system development, several CNV-associated disorders also lead to early developmental features involving other organ systems [3,4], including cardiac defects [5,6], kidney malformations[7], craniofacial features [3], and skeletal abnormalities [8]. For example, the 1q21.1 deletion causes variable expression of multiple neuronal and non-neuronal phenotypes, including developmental delay, autism, and schizophrenia as well as craniofacial features, cataracts, cardiac defects, and skeletal abnormalities [9–11]. Additionally, while the 7q11.23 deletion associated with Williams-Beuren syndrome (WBS) causes neuropsychiatric and behavioral features, other non-neuronal phenotypes, including supravalvular aortic stenosis, auditory defects, hypertension, diabetes mellitus, and musculoskeletal and connective tissue anomalies, are also observed among the deletion carriers [12].

Despite the notable prevalence of non-neuronal phenotypes in CNV carriers, functional studies of CNV genes have primarily focused on detailed assessments of neuronal and behavioral phenotypes in model systems. For example, mouse models for the 16p11.2 deletion exhibited post-natal lethality, reduced brain size and neural progenitor cell count, motor and habituation defects, synaptic defects, and behavioral defects [13–15]. Similarly, mouse models for the 3q29 deletion showed decreased weight and brain size, increased locomotor activity and startle response, and decreased spatial learning and memory [16,17]. However, fewer studies have focused on detailed evaluation of non-neuronal phenotypes in functional models of CNV disorders. For example, Arbogast and colleagues evaluated obesity and metabolic changes in

16p11.2 deletion mice, which showed reduced weight and impaired adipogenesis [18]. While Haller and colleagues showed that mice with knockdown of *MAZ*, a gene within the 16p11.2 deletion region, contribute to the genitourinary defects observed in individuals with the deletion [19], mouse studies on other homologs of 16p11.2 genes, including *TAOK2*, *KCTD13*, and *MAPK3*, have only focused on assessing neuronal defects [20–24]. Furthermore, Dickinson and colleagues reported a high-throughput analysis of essential genes in mice and identified both neuronal and non-neuronal phenotypes for individual gene knockouts, including more than 400 genes that lead to lethality [25]. While these efforts aided in implicating novel genes with human disease, our understanding of how genes associated with neurodevelopmental disorders contribute towards non-neuronal phenotypes is still limited. Therefore, a large-scale analysis of non-neuronal phenotypes is necessary to identify specific candidate genes within CNV regions and associated biological mechanisms that contribute towards these phenotypes.

Drosophila melanogaster is an excellent model system to evaluate homologs of neurodevelopmental genes, as many developmental processes and signaling pathways are conserved between humans and flies [26]. In fact, over 75% of human disease genes have homologs in *Drosophila*, including many genes involved in cellular signaling processes [27,28]. We recently examined the contributions of individual *Drosophila* homologs of 28 genes within the 16p11.2 and 3q29 deletion regions towards specific neurodevelopmental phenotypes, including rough eye phenotypes and defects in climbing ability, axon targeting, neuromuscular junction, and dendritic arborization [29,30]. While these findings implicated multiple genes within each CNV region towards conserved cellular processes in neuronal tissues, the conserved role of these genes in non-neuronal tissues is not well understood. The *Drosophila* wing is an effective model system to evaluate such developmental defects, as key components of conserved

signaling pathways, such as Notch, epidermal growth factor receptor (EGFR), Hegdehog, and Wnt pathways, were identified using fly wing models [31–37]. Although fly wing phenotypes cannot be directly translated to human phenotypes, defects observed in fly wings can be used to assess how homologs of human disease genes alter conserved cellular and developmental mechanisms. For example, Wu and colleagues showed that overexpression of the *Drosophila* homolog for *UBE3A*, associated with Angelman syndrome, leads to abnormal wing and eye morphology defects [38]. Furthermore, *Drosophila* mutant screens for developmental phenotypes, including wing defects, were used to identify conserved genes for several human genetic diseases, including Charcot-Marie-Tooth disease and syndromic microcephaly [39]. Kochinke and colleagues also recently performed a large-scale screening of ID-associated genes, and found an enrichment of wing trichome density and missing vein phenotypes in ID genes compared to control gene sets [40]. Hence, the fly wing provides a model system that is ideal for evaluating the contributions of individual homologs of CNV genes towards cellular and developmental defects.

In this study, we tested tissue-specific and cellular phenotypes of 79 fly homologs of human genes within ten pathogenic CNV regions and genes associated with neurodevelopmental disorders. Particularly, we used the adult fly wing to evaluate phenotypes in a non-neuronal tissue, and observed a wide range of robust qualitative and quantitative wing phenotypes among the 136 RNA interference (RNAi) lines tested in our study, including size defects, ectopic and missing veins, severe wrinkling, and lethality. Further analysis of cellular phenotypes revealed disruptions in conserved developmental processes in the larval imaginal wing disc, including altered levels of cell proliferation and apoptosis as well as altered expression patterns in the Wnt, Hedgehog, and Notch signaling pathways. However, we found no correlation in the severity of

106 phenotypes observed with wing and eye-specific knockdown. Our findings were further
107 supported by differences in expression patterns and network connectivity of human CNV genes
108 across different tissues. Our analysis emphasizes the importance of multiple genes within each
109 CNV region towards both global and tissue-specific developmental processes.

RESULTS

Knockdown of fly homologs of CNV genes contribute to a range of wing defects

Using an RNAi based analysis driven by the *bx*^{MS1096}*-GAL4* wing-specific driver, we tested a total of 136 RNAi lines for 59 homologs of genes within pathogenic CNV regions (chromosomal locations 1q21.1, 3q29, 7q11.23, 15q11.2, 15q13.3, 16p11.2, distal 16p11.2, 16p12.1, 16p13.11, and 17q12) and 20 homologs of genes associated with neurodevelopmental disorders (**Supp. Data 1**). Fly homologs of these genes were identified using the DIOPT orthology prediction tool [41]. We list both the human gene name and the fly gene name for each tested gene as *HUMAN GENE/Fly gene* (i.e. *KCTD13/CG10465*) as well as the human CNV region for context at first instance. We scored 20-25 adult wings for five distinct wing phenotypes in each non-lethal RNAi line, including wrinkled wing, discoloration, ectopic veins, missing veins, and bristle planar polarity phenotypes (**Fig. 1A; Supp. Data 2**). We first categorized each wing phenotype based on their severity and performed k-means clustering analysis to categorize each RNAi line by their overall phenotype severity (**Fig. 1B-C**). We observed four clusters of RNAi lines: 75 lines with no observable qualitative phenotypes (55.2%), 24 lines with mild phenotypes (17.7%), 10 lines with moderate phenotypes (7.4%), 21 lines with severe phenotypes (15.4%), and 6 lines with lethal phenotypes (4.4%), including *ACACA/ACC* within 17q12, *DLG1/dlg1* within 3q29, and *STX1A/Syx1A* within 7q11.23 (**Fig. 1B-D; Supp. Data 2**). We observed severe wrinkled wing phenotypes for 13/79 fly homologs, including *PPP4C/Pp4-19C* within 16p11.2, *ATXN2L/Atx2* within distal 16p11.2, *AATF/Aatf* within 17q12, and *MFI2/Tsf2* within 3q29 (**Fig. 2A-B, Supp. Data 3**). Interestingly, seven out of ten CNV regions contained at least one homolog that showed lethality or severe wing phenotypes, and five CNV regions (3q29, 16p11.2, distal 16p11.2, 16p12.1, and 17q12) had multiple homologs showing lethality or severe wing

phenotypes (**Fig. 2A, Supp. Data 3**). For example, RNAi lines for both *UQCRC2/UQCR-C2* and *POLR3E/Sin* within 16p12.1 showed lethality. Within the 3q29 region, *NCBP2/Cbp20* and *MFI2/Tsf2* showed severe phenotypes while *DLG1/dlg1* showed lethality. In contrast, 12/20 known neurodevelopmental genes showed no observable wing phenotypes, suggesting that these genes could be responsible for neuronal-specific phenotypes (**Fig. 2B, Supp. Data 3**). We note that 18/79 fly homologs showed discordant phenotypes between two or more RNAi lines for the same gene, which could be due to differences in expression of the RNAi construct among these lines (**Supp. Data 3**).

Certain qualitative phenotypes exhibited higher frequency in males compared to females. For example, discoloration (87 lines in males compared to 56 lines in females; $p=1.315\times10^{-4}$, two-tailed Fisher's exact test) and missing vein phenotypes (92 lines in males compared to 29 lines in females; $p=2.848\times10^{-16}$, two-tailed Fisher's exact test) at any degree of severity were more commonly observed in males than females (**Supp. Data 2**). In particular, 25/92 lines in males (compared to 1/29 in females) showed a total loss of the anterior crossvein (ACV) (**Supp. Data 2**). We further identified 17 RNAi lines that were lethal in males with wing-specific knockdown of fly homologs. While higher frequencies of wing phenotypes in males could be due to a sex-specific bias of developmental phenotypes, the increased severity we observed in males is most likely due to a stronger RNAi knockdown caused by an X-linked dosage compensation, as the *bx*^{MS1096}*-GAL4* driver is inserted on the fly X chromosome [42,43].

Next, we measured the total adult wing area and the lengths of six veins (longitudinal L2, L3, L4, L5, ACV, and posterior crossvein or PCV) in the adult wing for each of the tested RNAi lines that did not show lethality (or severe wrinkled phenotypes for vein length measurements) (**Fig. 3A**). Overall, we identified significant wing measurement changes for 89 RNAi lines

compared to controls, which included lines that did not have an observable qualitative wing phenotype (**Fig. 1D**). A summary of L3 vein lengths is presented in **Fig. 3B**, and the measurements for the remaining five veins are presented in **Supp. Figure 1** and **Supp. Data. 2**. We found that 33/61 of the homologs (54%) showed significant changes in L3 vein length, including 20 homologs with longer vein lengths and 13 homologs with shorter vein lengths (**Supp. Data 3**). Additionally, 41/74 of the fly homologs (55%) showed changes in wing area (**Supp. Data 3**), including 36 homologs which showed smaller wing areas and five homologs showed larger wing areas compared to controls (**Supp. Data 3**). For example, both homologs of genes within 1q21.1 region, *BCL9*/*lgs* and *FMO5/Fmo-2*, showed decreased wing area and vein length, potentially mirroring the reduced body length phenotype observed in mouse models of the deletion [44] (**Fig. 3B-C**). In addition, *PAK2/Pak* within 3q29, *TBX1/org-1* within 22q11.2, autism-associated *CHD8/kis*, and microcephaly-associated *ASPM/asp* also showed smaller wing areas and vein lengths (**Fig. 3B-C**). In contrast, *TRPM1/Trpm* within 15q13.3 and the cell proliferation gene *PTEN/Pten* [45] both showed larger wing areas and vein lengths (**Fig. 3B-C**). Furthermore, we identified eight homologs that showed no qualitative wing phenotypes but had significant changes in wing areas and vein lengths (**Supp. Data 3**), including *CCDC101/Sgf29* in distal 16p11.2, *FMO5/Fmo-2*, *TRPM1/Trpm*, *DHRS11/CG9150* in 17q12, and *NSUN5/Nsun5* in 7q11.23 (**Fig. 3B-C; Supp. Data 3**). These results indicate that homologs of certain CNV genes may influence variations in size without causing adverse wing phenotypes, and may be specifically implicated towards cellular growth mechanisms.

Homologs of CNV genes show global and tissue-specific effects during development

We previously showed that many of the same fly homologs of CNV genes that showed wing defects in the current study also contributed towards neuronal phenotypes in the fly eye [29,30], suggesting a role for these genes in global development. We therefore performed ubiquitous and eye-specific knockdown of fly homologs to assess tissue-specific effects in comparison to the wing phenotypes. First, we used the *da-GAL4* driver at 25°C to drive ubiquitous knockdown of RNAi lines for 31 homologs of CNV genes, including 19 that were previously published [29,30], and observed complete or partial lethality at larval and pupal stages with knockdown of 10/31 homologs (32.3%) (**Fig. 4A**). Lethal phenotypes have also been documented for 43/130 knockout mouse models of individual CNV genes as well as for the entire deletion (**Supp. Data 4**). For example, mouse models heterozygous for the 16p11.2 deletion showed partial neonatal lethality, while knockout mouse models of four individual genes within the 16p11.2 region, including *Ppp4C*$^{-/-}$ and *Kif22*$^{-/-}$, showed embryonic lethality [13,46,47]. In our study, the *DLG1/dlg1* line that showed lethality with wing-specific knockdown also exhibited larval lethality with ubiquitous knockdown, indicating its role in global development (**Fig. 4A**). In addition, six homologs that showed severe wing phenotypes also showed larval or pupal lethality with ubiquitous knockdown, including *ALDOA/Ald* and *PPP4C/Pp4-19C* within 16p11.2 and *ATXN2L/Atx2* and *TUFM/mEFTu1* within distal 16p11.2 (**Fig. 4A**). The remaining homologs that showed lethality with ubiquitous knockdown showed at least a mild qualitative or quantitative wing phenotype.

We next compared the phenotypes observed with wing-specific knockdown of fly homologs to their corresponding eye-specific knockdowns to evaluate tissue-specific effects. To quantitatively assess the phenotypic severity of cellular defects with eye-specific knockdown of

fly homologs, we developed a tool called *Flynotyper* [48] that determines the degree of disorganization among the ommatidia in the adult eye. We analyzed phenotypic scores obtained from *Flynotyper* for 66 RNAi lines of 45 fly homologs, including from previously-published datasets [29,30,48]. We found that 37/45 homologs (82.2%) exhibited both eye and wing-specific defects (**Fig. 4B, Supp. Fig. 2, Supp. Data 5**). Two homologs with significant eye phenotypes did not show any wing phenotypes, including *SPNS1/spin* within distal 16p11.2 and microcephaly-associated *SLC25A19/Tpc1* [49], while five homologs only showed wing-specific phenotypes, including *CDIPT/Pis* and *YPEL3/CG15309* within 16p11.2, *FBXO45/Fsn* and *OSTalpha/CG6836* within 3q29, and *UQCRC2/UQCR-C2* (**Fig. 4B, Supp. Fig. 2**). In particular, *UQCRC2/UQCR-C2* showed lethality with wing-specific knockdown, suggesting potential tissue-specific effects of this gene in non-neuronal cells (**Fig. 4B**). While most homologs contributed towards both eye and wing-specific phenotypes, we observed a wide range of severity in eye phenotypes that did not correlate with the severity of quantitative or qualitative wing phenotypes (**Fig. 4C**). For example, *TUFM/mEFTu1* showed a severe wing phenotype but only a mild increase in eye phenotypic score, while *SH2B1/Lnk*, also within the distal 16p11.2 region, showed severe rough eye phenotypes but only a mild increase in wing size (**Fig. 4D**). Similarly, *BCL9/lgs* also showed opposing tissue-specific effects with mild qualitative wing phenotype and severe eye phenotype, suggesting that the role of these homologs towards development differs across tissue types.

CNV genes show variable expression across different tissues in flies and humans

To assess how expression levels of CNV genes vary across different tissues, we first examined the expression patterns of fly homologs in larval and adult tissues using the FlyAtlas Anatomical

Microarray dataset [50]. We found that 76/77 homologs with available data were expressed in at least one larval and adult tissue (**Supp. Fig. 3, Supp. Data 6**). In general, we did not observe a correlation between wing phenotype severity and expression patterns of homologs in larval or adult tissues (**Fig. 5A**). For example, 58/77 homologs (75.3%) showed ubiquitous larval expression, including both fly homologs that showed no qualitative wing phenotypes, such as *KCTD13/CG10465* within 16p11.2 and *FBXO45/Fsn*, and those with severe wing phenotypes, such as *PPP4C/Pp4-19C* and *NCBP2/Cbp20* (**Fig. 5A, Supp. Fig. 3**). Furthermore, 30/39 homologs (76.9%) that showed eye phenotypes also had ubiquitous larval expression, providing further support to the observation that genes causing neuronal phenotypes may also contribute to developmental phenotypes in other tissues (**Supp. Data 5**). Of note, 9/77 homologs (11.7%) did not have any expression in the larval central nervous system, including *FMO5/Fmo-2*, *BDH1/CG8888* within 3q29, and *TBX6/Doc2* within 16p11.2 (**Fig. 5A, Supp. Fig. 3**). However, we observed wing phenotypes for 8/9 of these homologs, suggesting that they may contribute to tissue-specific phenotypes outside of the nervous system. Except for the epilepsy-associated *SCN1A/para* [51], which was exclusively expressed in both the larval central nervous system (CNS) and adult brain tissues, other tested neurodevelopmental genes were also expressed in non-neuronal tissues (**Fig. 5A**).

We further used the GTEx Consortium dataset [52] to examine tissue-specific expression of 150 human CNV and known neurodevelopmental genes across six tissues including brain, heart, kidney, lung, liver, and muscle. We found 121 genes that were expressed in at least one adult tissue, including 49 genes (32.7%) that showed ubiquitous expression across all six tissues (**Supp. Data 6**). Of the 112 genes expressed in non-neuronal tissues, 34 did not have any neuronal expression, including *TBX1*, *FMO5* and *GJA5* within 1q21.1, and *ATP2A1* within distal

16p11.2 (**Fig. 5B**, **Supp. Data 6**). *FMO5* and *TBX1* also showed non-neuronal expression in *Drosophila* tissues, suggesting that their tissue-specific expression is highly conserved (**Fig. 5A**). Other genes showing ubiquitous expression also had preferentially high expression for specific non-neuronal tissues, including *ALDOA* and *UQCRC2* for muscle and heart (**Fig. 5B**). In contrast, we found nine genes that were expressed only in the adult brain, including *FAM57B* and *DOC2A* within 16p11.2, as well as *SCN1A*, which showed similar CNS-only expression in *Drosophila* tissues (**Fig. 5B**, **Supp. Data 6**).

Knockdown of fly homologs of CNV genes lead to disruption of cellular processes

The disruption of basic cellular processes in neuronal cells, such as cell proliferation and apoptosis, have been implicated in neurodevelopmental disorders [53–55]. We previously identified defects in cell proliferation among photoreceptors neurons in larval eye discs with knockdown of 16p11.2 homologs, as well as increased apoptosis with knockdown of a subset of 3q29 homologs [29,30]. Here, we explored how these basic cellular processes are altered in non-neuronal cells, specifically in the developing wing disc, with knockdown of homologs of CNV genes. We targeted 27 fly homologs that showed a range of adult wing phenotypes for changes in cell proliferation and apoptosis, using anti-phospho-Histone H3 Ser10 (pH3) and anti-*Drosophila* caspase-1 (dcp1), respectively, in the third instar larval wing discs. We identified 23/27 homologs that showed significant increases in apoptotic cells compared to controls, including seven homologs, such as *PPP4C/Pp4-19C*, *ATXN2L/Atx2*, and *AATF/Aatf* , which showed dcp1 staining across the entire larval wing pouch (**Fig. 6A-B, Supp. Figs. 4-5, Supp. Data 7**). In addition, 16/27 genes showed decreased levels of proliferation, including eight homologs which also showed apoptosis defects, such as *CYFIP1/Sra-1* within 15q11.2,

SH2B1/Lnk, and the microcephaly gene *KIF11/Klp61F* (**Fig. 6A and 6C, Supp. Figs. 4-5, Supp. Data 7**). All six of the tested homologs with severe adult wing phenotypes showed both increased apoptosis and decreased proliferation (**Supp. Data 7**). Similarly, 3/4 homologs of genes showing lethality with wing-specific knockdown also showed defects in apoptosis or proliferation, with the exception of *ACACA/ACC* (**Supp. Figure 4**, **Supp. Data 7**). As $bx^{MS1096\text{-}GAL4}$ is located on the X-chromosome, we expected to see more severe defects in males compared with females with knockdown of homologs due to the X-linked dosage compensation [42,43]. However, knockdown of 3/11 tested homologs with sex-specific differences in adult wing phenotypes, including *BCL9/lgs*, *CYFIP1/Sra-1*, and *DNAJC30/CG11035* within 7q11.23, showed significantly decreased levels of cell proliferation in females but no change for males compared to their respective controls, suggesting a sex-specific effect of these genes for cell proliferation (**Supp. Fig. 5, Supp. Data 7**). Overall, our results suggest that cell proliferation and apoptosis are disrupted by reduced expression of homologs of CNV genes in both neuronal and non-neuronal tissues.

Knockdown of homologs of CNV genes disrupt conserved signaling pathways

Several conserved signaling pathways that are active in a spatial and temporal manner in the larval wing disc, such as Wnt, Hedgehog, BMP, and Notch signaling, regulate the anterior-posterior (A/P) and dorsal-ventral (D/V) boundaries to determine accurate morphology and vein patterning in the adult wing [36,37,56–58]. For example, Wnt and Notch signaling pathways both act along the D/V boundary to determine cell fate [59,60], while Hedgehog signaling is dependent upon expression of both engrailed in the posterior compartment and patched along the A/P border [61,62]. Furthermore, O'Roak and colleagues showed that genes identified from *de*

294 *novo* mutations in patients with autism are linked to β-catenin/Wnt pathway [63]. In addition,
295 familial loss-of-function mutations in the human hedgehog signaling pathway gene *PTCH1* are
296 implicated in basal cell nevus syndrome, leading to basal cell carcinoma [64,65].
297 Based on adult wing phenotypes and disruptions to cellular processes, we next tested
298 whether knockdown of 14 fly homologs disrupt conserved signaling pathways in the third instar
299 larval wing disc (**Supp. Data 7**). In particular, we evaluated the role of Wnt, Hedgehog, and
300 Notch signaling pathways by testing the expression patterns of four key proteins within these
301 pathways, including wingless (Wnt), patched (Hedgehog), engrailed (Hedgehog), and delta
302 (Notch). We found that 9/14 homologs, including 8/10 homologs showing severe wing
303 phenotypes or lethality, exhibited disruptions in at least one signaling pathway. For example, five
304 homologs with severe or lethal phenotypes showed disruptions of all four signaling pathways,
305 including *AATF/Aatf*, *NCBP2/Cbp20*, *POLR3E/Sin*, *PPP4C/Pp4-19C*, and *KIF11/Klp61F* (**Fig.**
306 **7, Supp. Data 7**). Our observations are in concordance with previous findings by Swarup and
307 colleagues, who showed that *PPP4C/Pp4-19C* is a candidate regulator of Wnt and Notch
308 signaling pathways in *Drosophila* larval wing discs [66]. Furthermore, two genes from the 3q29
309 region, *DLG1/dlg1* and *MFI2/Tsf2*, showed altered expression patterns for delta and patched but
310 not for engrailed, indicating that they selectively interact with the Hedgehog as well as Notch
311 signaling pathway (**Supp. Fig. 6**). In fact, Six and colleagues showed that Dlg1 directly binds to
312 the PDZ-binding domain of Delta1 [67]. In contrast, *ACACA/ACC* and *UQCRC2/UQCR-C2*
313 showed no changes in expression patterns for any of the four signaling proteins tested,
314 suggesting that the observed lethality could be due to other cellular mechanisms (**Supp. Fig. 6**).
315 We conclude that several homologs disrupt the expression of key proteins in signaling pathways

316 in the developing larval wing discs, potentially accounting for the developmental defects
317 observed in the adult wings.
318
319 **Connectivity patterns of CNV genes vary across human tissue-specific networks**
320 We examined patterns of connectivity for the nine candidate genes, based on the disruptions of
321 signaling pathways identified in the developing *Drosophila* wing discs, within the context of
322 human brain, heart, and kidney-specific gene interaction networks [68]. These tissue-specific
323 networks were constructed using Bayesian classifier-generated probabilities for pairwise genetic
324 interactions based on co-expression data [68]. We calculated the lengths of the shortest paths
325 between each candidate gene and 267 Wnt, Notch, and Hedgehog pathway genes in each
326 network as a proxy for connectivity (**Supp. Data 8**). In all three networks, each of the candidate
327 genes were connected to a majority of the tested signaling pathway genes (**Fig. 8A, Supp. Fig.**
328 **7**). Interestingly, we observed a higher connectivity (i.e. shorter path distances) between
329 candidate genes and Wnt and Hedgehog pathway genes in the brain-specific network compared
330 to the heart and kidney-specific networks (**Fig. 8B**). We further identified enrichments for genes
331 involved in specific biological processes among the connector genes that were located in the
332 shortest paths within neuronal and non-neuronal tissue-specific networks (**Fig. 8C, Supp. Data**
333 **8**). For example, axon-dendrite transport, dopaminergic signaling, and signal transduction
334 functions were enriched among connector genes only for the brain-specific network, while
335 organelle organization and protein ubiquitination were enriched among connector genes only for
336 kidney and heart networks (**Fig. 8C**). However, several core biological processes, such as cell
337 cycle, protein metabolism, transcriptional regulation, and RNA processing/splicing, were
338 enriched among connector genes within all three tissue-specific networks (**Fig. 8C**). Our analysis

339 highlights that human CNV genes potentially interact with developmental signaling pathways in
340 a ubiquitous manner, but may affect different biological processes in neuronal and non-neuronal
341 tissues.

DISCUSSION

We used the *Drosophila* wing as a model to assess how homologs of key CNV genes contribute towards non-neuronal phenotypes. We tested fly homologs of 79 genes and identified multiple homologs within each CNV region that exhibited strong phenotypes indicative of developmental disruptions. Several themes have emerged from our study highlighting the importance of fly homologs of CNV genes towards both global and tissue-specific phenotypes.

First, we found that fly homologs of CNV genes contribute towards developmental phenotypes through ubiquitous roles in neuronal and non-neuronal tissues. Although we did not study models for the entire CNV, nearly all individual fly homologs of CNV genes contribute to wing-specific developmental defects. It is likely that these genes may also contribute to additional phenotypes in other tissues that we did not assess. In fact, a subset of these homologs also showed early lethality with ubiquitous knockdown in addition to severe or lethal wing-specific phenotypes. However, we found no correlation between the severity of the eye and wing phenotypes, suggesting tissue-specific effects of these homologs towards developmental defects. In contrast, fly homologs of known neurodevelopmental genes generally showed milder wing phenotypes compared with eye phenotypes, indicating a more neuronal role for these genes. While our study only examined a subset of CNV genes with *Drosophila* homologs, phenotypic data from knockout mouse models also support a global developmental role for individual CNV genes. In fact, 44/130 knockout models of CNV genes within the Mouse Genome Informatics (MGI) database [69] exhibited non-neuronal phenotypes, including 20 homologs of CNV genes that showed both neuronal and non-neuronal phenotypes (**Supp. Data 4**). For example, knockout mouse models of *Dlg1*$^{-/-}$ show defects in dendritic growth and branching in the developing nervous system, in addition to craniofacial features and multiple kidney and urinary tract defects

365 [70–73]. Furthermore, Chapman and colleagues showed that knockout of *Tbx6*$^{-/-}$ caused defects
366 in mesodermal and neuronal differentiation early in development, leading to abnormal vascular,
367 tail bud, and neural tube morphology [74]. These observations further support our findings that
368 most fly homologs of CNV genes have a global role in development that could account for the
369 observed non-neuronal defects.

370 *Second*, based on tissue-specific phenotypes, we identified fly homologs of CNV genes
371 that are key regulators of conserved cellular processes important for development. For example,
372 9/10 homologs with severe or lethal adult wing phenotypes also exhibited defects in cell
373 proliferation and apoptosis during development. In fact, we found concordance between cellular
374 processes affected by wing and eye-specific knockdown of homologs of genes within 16p11.2
375 and 3q29 regions, including decreased proliferation for *MAPK3/rl* and increased apoptosis for
376 *NCBP2/Cbp20* and *DLG1/dlg1* [29,30]. While eye-specific knockdown of *BDH1/CG8888*
377 showed decreased cell proliferation in larval eye discs [30], we found increased cell proliferation
378 with wing-specific knockdown, suggesting a tissue-specific effect for this gene. Notably, at least
379 one fly homolog per CNV region showed defects in cell proliferation or apoptosis, suggesting
380 these cellular processes are important for development in both neuronal and non-neuronal
381 tissues. For example, *ATXN2L/Atx2*, *SH2B1/Lnk*, and *CCDC101/Sgf29* each showed decreased
382 proliferation and increased apoptosis, suggesting a potential shared cellular mechanism for
383 several genes within the distal 16p11.2 deletion. Furthermore, a subset of these genes also
384 disrupted multiple signaling pathways, indicating a potential role for these homologs as key
385 regulators of developmental processes. We specifically identified five homologs whose
386 knockdown caused disruptions of Wnt, Notch, and hedgehog signaling pathways. Each of these
387 genes have important roles in cell cycle regulation, apoptosis, transcription, or RNA processing,

388 based on Gene Ontology annotations [75,76]. In fact, we found that the RNA transport protein
389 *NCBP2/Cbp20* [77], which we recently identified as a key modifier gene for the 3q29 deletion
390 [30], interfaced with all three signaling pathways. Furthermore, *AATF* disrupts apoptosis and
391 promotes cell cycle progression through displacement of HDAC1 [78–80], while *PPP4C*
392 promotes spindle organization at the centromeres during mitosis [81]. While we only evaluated
393 the role of these genes towards development in a single fly tissue, our additional analysis of
394 human gene interaction networks showed strong connectivity between the CNV genes and
395 signaling pathways in multiple neuronal and non-neuronal human tissues. In fact, cell cycle
396 genes were enriched among the connector genes in all three tissue-specific networks, further
397 emphasizing the role of cell cycle processes towards developmental phenotypes. Notably, we
398 also observed certain biological processes enriched among connector genes that were specific to
399 neuronal or non-neuronal tissues, indicating that genes within CNV regions may affect different
400 biological processes in a tissue-specific manner.

401 *Overall*, we show that fly homologs of most CNV genes contribute towards global
402 developmental phenotypes, although exactly how they contribute toward such phenotypes varies
403 between neuronal and non-neuronal tissues. Previous functional studies for CNV disorders have
404 focused primarily on identifying candidate genes for the observed neuronal phenotypes. In this
405 study, we identified several homologs of CNV genes that are responsible for non-neuronal
406 defects, as well as novel associations between these homologs and conserved biological
407 processes and pathways. We therefore propose that multiple genes within each CNV region
408 differentially disrupt conserved cellular pathways and biological processes in neuronal versus
409 non-neuronal tissues during development (**Fig. 9**). These results are in line with a multigenic
410 model for CNV disorders, as opposed to models where individual causative genes are

411 responsible for specific phenotypes [29,30,82]. Our study further exemplifies the utility of
412 evaluating non-neuronal phenotypes in addition to neuronal phenotypes in functional models of
413 individual genes and CNV regions associated with developmental disorders, including future
414 studies in mammalian or cellular model systems. Further studies exploring how CNV genes
415 interact with each other and with other developmental pathways could more fully explain the
416 conserved mechanisms underlying global developmental defects and identify potential
417 therapeutic targets for these disorders.
418

MATERIALS AND METHODS

Fly stocks and genetics

We tested 59 *Drosophila* homologs for 130 human genes that span across 10 pathogenic CNV regions associated with neurodevelopmental disorders (1q21.1, 3q29, 7q11.23, 15q11.2, 15q13.3, 16p11.2, distal 16p11.2, 16p12.1, 16p13.11, and 17q12) [83] (**Supp. Data 1**). In addition, we evaluated fly homologs of 20 human genes known to be in involved in neurodevelopmental disorders [48,84] (**Supp. Data 1**). These include genes involved in beta-catenin signaling pathway (5 genes), core genes implicated in neurodevelopmental disorders (8 genes), and genes associated with microcephaly (7 genes) [85]. We used the DRSC Integrative Ortholog Prediction Tool (DIOPT, v.7.1) to identify the fly homologs for each human gene [41] (**Supp. Data 1**).

To knockdown individual genes in specific tissues, we used RNA interference (RNAi) and the *UAS-GAL4* system (**Fig. 1A**), a well-established tool that allows for tissue-specific expression of a gene of interest [86]. RNAi lines were obtained from Vienna *Drosophila* Resource Center (VDRC) that include both GD and KK lines. We tested a total of 136 lines in our final data analysis (**Supp. Data 9**), after eliminating KK lines with additional insertion that drives the overexpression of the Tiptop (*tio*) transcription factor [87,88]. A complete list of stock numbers and full genotypes for all RNAi lines used in this study is presented in **Supp. Data 9**. We used the bx^{MS1096}*-GAL4/FM7c;;UAS-Dicer2/TM6B* driver for wing-specific knockdown and w^{1118}*;GMR-GAL4;UAS-Dicer2* driver (Claire Thomas, Penn State University) for eye-specific knockdown of RNAi lines. Ubiquitous knockdown experiments were performed using the *w;da-GAL4;+* driver (Scott Selleck, Penn State University). For all experiments, we used appropriate GD (w^{1118}, VDRC# 60000) or KK (y,w^{1118}*; P{attP,*y^{+}*,*$w^{3`}$*}*, VDRC# 60100) lines as controls to compare against lines with knockdown of individual homologs. All fly lines were reared on

standard yeast *Drosophila* medium at room temperature. All crosses were set and maintained at 25°C, except for the eye knockdown experiments which were maintained at 30°C.

Phenotypic analysis of adult wing images

Adult progeny were isolated from crosses between RNAi lines and *bx*^{MS1096}*-GAL4* driver shortly after eclosion, and kept at 25°C until day 2-5 (**Fig. 1A**). At that point, the progeny were frozen at -80°C, and were then moved to -20°C prior to imaging and storage. Approximately 20-25 progeny, both male and female, were collected for each RNAi line tested. The adult wings were plucked from frozen flies and mounted on a glass slide. The slides were covered with a coverslip and sealed using clear nail polish. Adult wing images were captured using a Zeiss Discovery V20 stereoscope (Zeiss, Thornwood, NY, USA), with a ProgRes Speed XT Core 3 camera and CapturePro v.2.8.8 software (Jenoptik AG, Jena, Germany) at 40X magnification.

For each non-lethal RNAi line, we scored the adult wing images for five qualitative phenotypes, including wrinkled wing, discoloration, missing veins, ectopic veins, and bristle planar polarity defects, on a scale of 1 (no phenotype) to 5 (lethal) (**Fig. 2C**). Lines showing severely wrinkled wings or lethality were scored as 4 (severe) or 5 (lethal) for all five phenotypes. We calculated the frequency of each phenotypic score (i.e. mild bristle polarity, moderate discoloration) across all of the wing images for each line (**Fig. 2A-B**), and then performed k-means clustering of these values to generate five clusters for overall wing phenotypes (**Fig. 1C**). For quantitative analysis of wing phenotypes, we used the Fiji ImageJ software [89] to calculate the wing area using the Measure Area tool, and calculated the lengths of longitudinal veins L2, L3, L4, and L5 as well as the anterior and posterior crossveins (ACV and PCV), by tracing individual veins using the Segmented Line tool (**Fig. 3A, Supp. Data 2**).

We determined discordant homologs when RNAi lines for the same homologs showed inconsistent wing phenotypes. For each homolog with multiple RNAi lines, we checked discordance among RNAi lines for no phenotype versus any qualitative or quantitative phenotypes, followed by discordance for small or large wing measurement phenotypes (**Supp. Data 3**).

Phenotypic analysis of adult eye images

We crossed RNAi lines with *GMR-GAL4* to achieve eye-specific knockdown of homologs of CNV and known neurodevelopmental genes. Adult 2-3-day old female progenies from the crosses were collected, immobilized by freezing at -80°C, and then moved to -20°C prior to imaging and storage. Flies were mounted on Blu-tac (Bostik Inc, Wauwatosa, WI, USA) and imaged using an Olympus BX53 compound microscope with LMPLan N 20X air objective using a DP73 c-mount camera at 0.5X magnification (Olympus Corporation, Tokyo, Japan). CellSens Dimension software (Olympus Corporation, Tokyo, Japan) was used to capture the eye images, which were then stacked using the Zerene Stacker software (Zerene Systems LLC, Richland, WA, USA). All eye images presented in this study are maximum projections of 20 consecutive optical z-sections, at a z-step size of 12.1μm. Finally. we used our computational method called *Flynotyper* (https://flynotyper.sourceforge.net) to quantify the degree of rough eye phenotypes present due to knockdown of homologs of CNV or neurodevelopmental genes [48]. *Flynotyper* scores for homologs of 16p11.2 and 3q29, as well as select core neurodevelopmental genes, were derived from our previous studies [29,30,48].

488 **Immunohistochemistry**

489 Wing imaginal discs from third instar larvae were dissected in 1X PBS. The tissues were fixed
490 using 4% paraformaldehyde and blocked using 1% bovine serum albumin (BSA). The wing discs
491 were incubated with primary antibodies using appropriate dilutions overnight at 4°C. We used
492 the following primary antibodies: mouse monoclonal anti-pHistone3 (S10) (1:100 dilutions, Cell
493 Signaling 9706L), rabbit polyclonal anti-cleaved *Drosophila* Dcp1 (Asp216) (1:100 dilutions,
494 Cell Signaling 9578S), mouse monoclonal anti-Wingless (1:200 dilutions, DSHB, 4D4), mouse
495 monoclonal anti-Patched (1:50 dilutions, DSHB, *Drosophila* Ptc/APA1), mouse monoclonal
496 anti-Engrailed (1:50 dilutions, DSHB, 4D9), and mouse monoclonal anti-Delta (1:50 dilutions,
497 DSHB, C594.9B). Following incubation with primary antibodies, the wing discs were washed
498 and incubated with secondary antibodies at 1:200 dilution for two hours at room temperature.
499 We used the following secondary antibodies: Alexa Fluor 647 dye goat anti-mouse (A21235,
500 Molecular Probes by Invitrogen/Life Technologies), Alexa Fluor 568 dye goat anti-rabbit
501 (A11036, Molecular Probes by Invitrogen/Life Technologies), and Alexa Fluor 568 dye goat
502 anti-mouse (A11031, Molecular Probes by Invitrogen/Life Technologies). All washes and
503 antibody dilutions were made using 0.3% PBS with Triton-X.

504 Third instar larvae wing imaginal discs were mounted in Prolong Gold antifade reagent
505 with DAPI (Thermo Fisher Scientific, P36930) for imaging using an Olympus Fluoview FV1000
506 laser scanning confocal microscope (Olympus America, Lake Success, NY). Images were
507 acquired using FV10-ASW 2.1 software (Olympus, Waltham, MA, USA). Composite z-stack
508 images were analyzed using the Fiji ImageJ software [89]. To calculate the number of pH3
509 positive cells within the wing pouch area of the wing discs, we used the AnalyzeParticles
510 function in ImageJ, while manual counting was used to quantify Dcp1 positive cells. We note

that cell proliferation and apoptosis staining for *NCBP2/Cbp20*, *DLG1/dlg1*, *BDH1/CG8888*, and *FBXO45/Fsn* were previously published[30].

Statistical analysis

Significance for the wing area and vein length measurements, cell counts for proliferation and apoptosis, and *Flynotyper* scores were compared to appropriate GD or KK controls using one-tailed or two-tailed Mann-Whitney tests. P-values for each set of experiments were corrected for multiple testing using Benjamini-Hochberg correction. All statistical and clustering analysis was performed using R v.3.6.1 (R Center for Statistical Computing, Vienna, Austria). Details for the statistical tests performed for each dataset are provided in **Supp. Data 10**.

Expression data analysis

We obtained tissue-specific expression data for fly homologs of CNV genes from the FlyAtlas Anatomical Microarray dataset [50]. Raw FPKM (fragments per kilobase of transcript per million reads) expression values for each tissue were categorized as follows: <10, no expression; 10-100, low expression; 100-500, moderate expression; 500-1000, high expression; and >1000, very high expression (**Supp. Data 6**). The median expression among midgut, hindgut, Malpighian tube, and (for adult only) crop tissues was used to represent the overall gut expression. We similarly obtained human tissue-specific expression data for CNV genes from the GTEx Consortium v.1.2 RNA-Seq datasets [52]. Median TPM (transcripts per million reads) expression values for each tissue were categorized as follows: <3, no expression; 3-10, low expression; 10-25, moderate expression; 25-100, high expression; and >100, very high expression (**Supp. Data 6**). The median expression among all brain and heart sub-tissues was

used to represent brain and heart expression, while the median expression among all colon, esophagus, small intestine, and stomach sub-tissues was used to represent digestive tract expression. Preferential gene expression for a particular tissue within the GTEx dataset was determined if the expression values for that tissue were greater than the third quartile of all tissue expression values for that gene, plus 1.5 times the interquartile range. Venn diagrams were generated using the Venny webtool (http://bioinfogp.cnb.csic.es/tools/venny) (**Supp. Fig. 3**).

Network analysis

We obtained human tissue-specific gene interaction networks for brain, heart, and kidney tissues from the GIANT network database [68] within HumanBase (https://hb.flatironinstitute.org). These networks were built by training a Bayesian classifier based on tissue-specific gene co-expression datasets, which then assigned a posterior probability for interactions between each pair of genes within the genome for a particular tissue. We downloaded the "Top edge" version of each tissue-specific network, and extracted all gene pairs with posterior probabilities >0.2 to create sub-networks containing the top ~0.5% tissue-specific interactions. Next, we identified the shortest paths in each sub-network between human CNV genes whose fly homologs disrupted signaling pathways in the larval wing disc and human genes within each disrupted pathway, using the inverse of the posterior probability as weights for each edge in the network. Gene sets from the human Notch (KEGG:map04330), Wnt (KEGG:map04310) and Hedgehog pathways (KEGG:map04340) were curated from the Kyoto Encyclopedia of Genes and Genomes (KEGG) pathway database [90]. Using the NetworkX Python package [91], we calculated the shortest distance between each CNV gene and pathway gene, and identified connecting genes that were within each of the shortest paths for the three tissue-specific networks. We further tested for

557 enrichment of Gene Ontology (GO) terms (PantherDB GO-Slim) among the connector genes
558 using the PantherDB Gene List Analysis tool [92]. Lists of the shortest paths and connector
559 genes in each tissue-specific network, as well as enriched GO terms for sets of connector genes,
560 are provided in **Supp. Data 8**. Gene networks were visualized using Cytoscape v.3.7.2 [93]
561 using an edge-weighted spring embedded layout.
562

DATA AVAILABILITY

All data supporting the findings of this study are available within the paper and its supplementary information files.

CODE AVAILABILITY

All source code for data analysis in this manuscript, including scripts for k-means clustering of fly phenotypes and network connectivity of CNV and developmental pathway genes, are available on the Girirajan lab GitHub page at https://github.com/girirajanlab/CNV_wing_project.

ACKNOWLEDGEMENTS

The authors thank Drs. Scott Selleck and Claire Thomas for providing fly lines for the experiments, and members of the Girirajan Lab for their helpful discussions and comments on the manuscript. This work was supported by NIH R01-GM121907 and resources from the Huck Institutes of the Life Sciences to S.G., and NIH T32-GM102057 to M.J.

CONTRIBUTIONS

T.Y., M.J., S.Y., and S.G. designed the study. T.Y., S.Y., L.P., S.K., D.J.G., A.S., Y.M., J.I., and Z.C.L. performed the functional experiments. T.Y. and M.J. performed the expression and network experiments. T.Y., M.J., and S.G. analyzed the data and wrote the manuscript with input from all authors.

COMPETING OF INTERESTS

The authors declare that they have no competing interests.

REFERENCES

1. Girirajan S, Campbell CD, Eichler EE. Human Copy Number Variation and Complex Genetic Disease. Annu Rev Genet. 2011;45: 203–226. doi:10.1146/annurev-genet-102209-163544
2. Malhotra D, Sebat J. CNVs: harbingers of a rare variant revolution in psychiatric genetics. Cell. 2012;148: 1223–1241. doi:10.1016/j.cell.2012.02.039
3. Cooper GM, Coe BP, Girirajan S, Rosenfeld JA, Vu TH, Baker C, et al. A copy number variation morbidity map of developmental delay. Nat Genet. 2011;43: 838–846. doi:10.1038/ng.909
4. Zhang F, Gu W, Hurles ME, Lupski JR. Copy Number Variation in Human Health, Disease, and Evolution. Annu Rev Genomics Hum Genet. 2009;10: 451–481. doi:10.1146/annurev.genom.9.081307.164217
5. Greenway SC, Pereira AC, Lin JC, Depalma SR, Israel SJ, Mesquita SM, et al. De novo copy number variants identify new genes and loci in isolated sporadic tetralogy of Fallot. Nat Genet. 2009;41: 931–935. doi:10.1038/ng.415
6. Glessner JT, Bick AG, Ito K et al. Increased Frequency of De Novo Copy Number Variations in Congenital Heart Disease by Integrative Analysis of SNP Array and Exome Sequence Data. Circ Res. 2014;115: 884–896. doi:10.1161/CIRCRESAHA.115.304458.
7. Sanna-Cherchi S, Kiryluk K, Burgess KE, Bodria M, Sampson MG, Hadley D, et al. Copy-number disorders are a common cause of congenital kidney malformations. Am J Hum Genet. 2012;91: 987–997. doi:10.1016/j.ajhg.2012.10.007
8. Zahnleiter D, Uebe S, Ekici AB, Hoyer J, Wiesener A, Wieczorek D, et al. Rare copy number variants are a common cause of short stature. PLoS Genet. 2013;9: e1003365. doi:10.1371/journal.pgen.1003365
9. Mefford HC, Sharp AJ, Baker C, Itsara A, Jiang Z, Buysse K, et al. Recurrent rearrangements of chromosome 1q21.1 and variable pediatric phenotypes. N Engl J Med. 2008;359: 1685–99. doi:10.1056/NEJMoa0805384
10. Brunetti-Pierri N, Berg JS, Scaglia F, Belmont J, Bacino CA, Sahoo T, et al. Recurrent reciprocal 1q21.1 deletions and duplications associated with microcephaly or macrocephaly and developmental and behavioral abnormalities. Nat Genet. 2008;40: 1466–1471. doi:10.1038/ng.279
11. Christiansen J, Dyck JD, Elyas BG, Lilley M, Bamforth JS, Hicks M, et al. Chromosome 1q21.1 contiguous gene deletion is associated with congenital heart disease. Circ Res. 2004;94: 1429–35. doi:10.1161/01.RES.0000130528.72330.5c
12. Pober BR. Williams-Beuren syndrome. N Engl J Med. 2010;362: 239–52. doi:10.1056/NEJMra0903074
13. Horev G, Ellegood J, Lerch JP, Son Y-EE, Muthuswamy L, Vogel H, et al. Dosage-dependent phenotypes in models of 16p11.2 lesions found in autism. Proc Natl Acad Sci. 2011;108: 17076–17081. doi:10.1073/pnas.1114042108
14. Pucilowska J, Vithayathil J, Tavares EJ, Kelly C, Karlo JC, Landreth GE. The 16p11.2 Deletion Mouse Model of Autism Exhibits Altered Cortical Progenitor Proliferation and Brain Cytoarchitecture Linked to the ERK MAPK Pathway. J Neurosci. 2015;35: 3190–3200. doi:10.1523/JNEUROSCI.4864-13.2015
15. Portmann T, Yang M, Mao R, Panagiotakos G, Ellegood J, Dolen G, et al. Behavioral

abnormalities and circuit defects in the basal ganglia of a mouse model of 16p11.2 deletion syndrome. Cell Rep. 2014;7: 1077–1092. doi:10.1016/j.celrep.2014.03.036

16. Rutkowski TP, Purcell RH, Pollak RM, Grewenow SM, Gafford GM, Malone T, et al. Behavioral changes and growth deficits in a CRISPR engineered mouse model of the schizophrenia-associated 3q29 deletion. Mol Psychiatry. 2019. doi:10.1038/s41380-019-0413-5
17. Baba M, Yokoyama K, Seiriki K, Naka Y, Matsumura K, Kondo M, et al. Psychiatric-disorder-related behavioral phenotypes and cortical hyperactivity in a mouse model of 3q29 deletion syndrome. Neuropsychopharmacology. 2019;44: 2125–2135. doi:10.1038/s41386-019-0441-5
18. Arbogast T, Ouagazzal A-M, Chevalier C, Kopanitsa M, Afinowi N, Migliavacca E, et al. Reciprocal Effects on Neurocognitive and Metabolic Phenotypes in Mouse Models of 16p11.2 Deletion and Duplication Syndromes. PLOS Genet. 2016;12: e1005709. doi:10.1371/journal.pgen.1005709
19. Haller M, Au J, O'Neill M, Lamb DJ. 16p11.2 transcription factor MAZ is a dosage-sensitive regulator of genitourinary development. Proc Natl Acad Sci. 2018;115: 201716092. doi:10.1073/pnas.1716092115
20. Yadav S, Oses-Prieto JA, Peters CJ, Zhou J, Pleasure SJ, Burlingame AL, et al. TAOK2 Kinase Mediates PSD95 Stability and Dendritic Spine Maturation through Septin7 Phosphorylation. Neuron. 2017;93: 379–393. doi:10.1016/j.neuron.2016.12.006
21. Richter M, Murtaza N, Scharrenberg R, White SH, Johanns O, Walker S, et al. Altered TAOK2 activity causes autism-related neurodevelopmental and cognitive abnormalities through RhoA signaling. Mol Psychiatry. 2019;24: 1329–1350. doi:10.1038/s41380-018-0025-5
22. Golzio C, Willer J, Talkowski ME, Oh EC, Taniguchi Y, Jacquemont S, et al. KCTD13 is a major driver of mirrored neuroanatomical phenotypes of the 16p11.2 copy number variant. Nature. 2012;485: 363–367. doi:10.1038/nature11091
23. Escamilla CO, Filonova I, Walker AK, Xuan ZX, Holehonnur R, Espinosa F, et al. Kctd13 deletion reduces synaptic transmission via increased RhoA. Nature. 2017;551: 227–231. doi:10.1038/nature24470
24. Ip JPK, Nagakura I, Petravicz J, Li K, Wiemer EAC, Sur M. Major vault protein, a candidate gene in 16p11.2 microdeletion syndrome, is required for the homeostatic regulation of visual cortical plasticity. J Neurosci. 2018;38: 2017–2034. doi:10.1523/JNEUROSCI.2034-17.2018
25. Dickinson ME, Flenniken AM, Ji X, Teboul L, Wong MD, White JK, et al. High-throughput discovery of novel developmental phenotypes. Nature. 2016;537: 508–514. doi:10.1038/nature19356
26. Wangler MF, Yamamoto S, Bellen HJ. Fruit flies in biomedical research. Genetics. 2015;199: 639–653. doi:10.1534/genetics.114.171785
27. Chien S. Homophila: human disease gene cognates in Drosophila. Nucleic Acids Res. 2002;30: 149–151. doi:10.1093/nar/30.1.149
28. Reiter LT, Potocki L, Chien S, Gribskov M, Bier E. A systematic analysis of human disease-associated gene sequences in Drosophila melanogaster. Genome Res. 2001;11: 1114–1125. doi:10.1101/gr.169101
29. Iyer J, Singh MD, Jensen M, Patel P, Pizzo L, Huber E, et al. Pervasive genetic

interactions modulate neurodevelopmental defects of the autism-Associated 16p11.2 deletion in Drosophila melanogaster. Nat Commun. 2018;9: 2548. doi:10.1038/s41467-018-04882-6

30. Singh MD, Jensen M, Lasser M, Huber E, Yusuff T, Pizzo L, et al. NCBP2 modulates neurodevelopmental defects of the 3q29 deletion in Drosophila and X. laevis models. bioRxiv. 2019; 614750. doi:10.1101/614750

31. Molnar C, Resnik-Docampo M, F. M, Martin M, F. C, de Celis JF. Signalling Pathways in Development and Human Disease: A Drosophila Wing Perspective. Human Genetic Diseases. InTech; 2011. doi:10.5772/23858

32. Dworkin I, Gibson G. Epidermal growth factor receptor and transforming growth factor-β signaling contributes to variation for wing shape in Drosophila melanogaster. Genetics. 2006;173: 1417–1431. doi:10.1534/genetics.105.053868

33. Testa ND, Dworkin I. The sex-limited effects of mutations in the EGFR and TGF-β signaling pathways on shape and size sexual dimorphism and allometry in the Drosophila wing. Dev Genes Evol. 2016;226: 159–171. doi:10.1007/s00427-016-0534-7

34. Yan SJ, Gu Y, Li WX, Fleming RJ. Multiple signaling pathways and a selector protein sequentially regulate Drosophila wing development. Development. 2004;131: 285–298. doi:10.1242/dev.00934

35. Strigini M, Cohen SM. A Hedgehog activity gradient contributes to AP axial patterning of the Drosophila wing. Development. 1997;124: 4697–4705.

36. Diaz de la Loza MC, Thompson BJ. Forces shaping the Drosophila wing. Mech. Dev. 2017;144: 23–32. doi:10.1016/j.mod.2016.10.003

37. Bier E. Drosophila, the golden bug, emerges as a tool for human genetics. Nat Rev Genet. 2005;6: 9–23. doi:10.1038/nrg1503

38. Wu Y, Bolduc F V, Bell K, Tully T, Fang Y, Sehgal A, et al. A Drosophila model for Angelman syndrome. Proc Natl Acad Sci U S A. 2008;105: 12399–12404. doi:10.1073/pnas.0805291105

39. Yamamoto S, Jaiswal M, Charng WL, Gambin T, Karaca E, Mirzaa G, et al. A drosophila genetic resource of mutants to study mechanisms underlying human genetic diseases. Cell. 2014;159: 200–214. doi:10.1016/j.cell.2014.09.002

40. Kochinke K, Zweier C, Nijhof B, Fenckova M, Cizek P, Honti F, et al. Systematic Phenomics Analysis Deconvolutes Genes Mutated in Intellectual Disability into Biologically Coherent Modules. Am J Hum Genet. 2016;98: 149–164. doi:10.1016/j.ajhg.2015.11.024

41. Hu Y, Flockhart I, Vinayagam A, Bergwitz C, Berger B, Perrimon N, et al. An integrative approach to ortholog prediction for disease-focused and other functional studies. BMC Bioinformatics. 2011;12: 357. doi:10.1186/1471-2105-12-357

42. Capdevila J, Guerrero I. Targeted expression of the signaling molecule decapentaplegic induces pattern duplications and growth alterations in Drosophila wings. EMBO J. 1994;13: 4459–4468. doi:10.1002/j.1460-2075.1994.tb06768.x

43. Lindström R, Lindholm P, Palgi M, Saarma M, Heino TI. In vivo screening reveals interactions between Drosophila Manf and genes involved in the mitochondria and the ubiquinone synthesis pathway. BMC Genet. 2017;18: 52. doi:10.1186/s12863-017-0509-3

44. Nielsen J, Fejgin K, Sotty F, Nielsen V, Mørk A, Christoffersen CT, et al. A mouse model of the schizophrenia-associated 1q21.1 microdeletion syndrome exhibits altered

mesolimbic dopamine transmission. Transl Psychiatry. 2017;7: 1261. doi:10.1038/s41398-017-0011-8

45. Huang H, Potter CJ, Tao W, Li DM, Brogiolo W, Hafen E, et al. PTEN affects cell size, cell proliferation and apoptosis during Drosophila eye development. Development. 1999;126: 5365–5372. doi:10.5167/uzh-627

46. Toyo-oka K, Mori D, Yano Y, Shiota M, Iwao H, Goto H, et al. Protein phosphatase 4 catalytic subunit regulates Cdk1 activity and microtubule organization via NDEL1 dephosphorylation. J Cell Biol. 2008;180: 1133–1147. doi:10.1083/jcb.200705148

47. Ohsugi M, Adachi K, Horai R, Kakuta S, Sudo K, Kotaki H, et al. Kid-Mediated Chromosome Compaction Ensures Proper Nuclear Envelope Formation. Cell. 2008;132: 771–782. doi:10.1016/j.cell.2008.01.029

48. Iyer J, Wang Q, Le T, Pizzo L, Grönke S, Ambegaokar SS, et al. Quantitative assessment of eye phenotypes for functional genetic studies using Drosophila melanogaster. G3 Genes, Genomes, Genet. 2016;6: 1427–1437. doi:10.1534/g3.116.027060

49. Rosenberg MJ, Agarwala R, Bouffard G, Davis J, Fiermonte G, Hilliard MS, et al. Mutant deoxynucleotide carrier is associated with congenital microcephaly. Nat Genet. 2002;32: 175–179. doi:10.1038/ng948

50. Chintapalli VR, Wang J, Dow JAT. Using FlyAtlas to identify better Drosophila melanogaster models of human disease. Nat. Genet. 2007;39: 715–720. doi:10.1038/ng2049

51. Claes L, Del-Favero J, Ceulemans B, Lagae L, Van Broeckhoven C, De Jonghe P. De novo mutations in the sodium-channel gene SCN1A cause severe myoclonic epilepsy of infancy. Am J Hum Genet. 2001;68: 1327–1332. doi:10.1086/320609

52. Ardlie KG, DeLuca DS, Segrè A V., Sullivan TJ, Young TR, Gelfand ET, et al. The Genotype-Tissue Expression (GTEx) pilot analysis: Multitissue gene regulation in humans. Science. 2015;348: 648–660. doi:10.1126/science.1262110

53. Ernst C. Proliferation and Differentiation Deficits are a Major Convergence Point for Neurodevelopmental Disorders. Trends Neurosci. 2016;39: 290–299. doi:10.1016/j.tins.2016.03.001

54. Marchetto MC, Belinson H, Tian Y, Freitas BC, Fu C, Vadodaria KC, et al. Altered proliferation and networks in neural cells derived from idiopathic autistic individuals. Mol Psychiatry. 2017;22: 820–835. doi:10.1038/mp.2016.95

55. Wei H, Alberts I, Li X. The apoptotic perspective of autism. Int J Dev Neurosci. 2014;36: 13–18. doi:10.1016/j.ijdevneu.2014.04.004

56. Hartl TA, Scott MP. Wing tips: The wing disc as a platform for studying Hedgehog signaling. Methods. 2014;68: 199–206. doi:10.1016/j.ymeth.2014.02.002

57. de Celis JF, García-Bellido A. Roles of the Notch gene in Drosophila wing morphogenesis. Mech Dev. 1994;46: 109–122. doi:10.1016/0925-4773(94)90080-9

58. Raftery LA, Umulis DM. Regulation of BMP activity and range in Drosophila wing development. Curr Opin Cell Biol. 2012;24: 158–65. doi:10.1016/j.ceb.2011.11.004

59. Diaz-Benjumea FJ, Cohen SM. Serrate signals through Notch to establish a Wingless-dependent organizer at the dorsal/ventral compartment boundary of the Drosophila wing. Development. 1995;121: 4215–4225.

60. Becam I, Milán M. A permissive role of Notch in maintaining the DV affinity boundary of the Drosophila wing. Dev Biol. 2008;322: 190–198. doi:10.1016/j.ydbio.2008.07.028

766 61. Zecca M, Basler K, Struhl G. Sequential organizing activities of engrailed, hedgehog and
767 decapentaplegic in the Drosophila wing. Development. 1995;121: 2265–2278.
768 doi:10.5167/uzh-1053
769 62. Tabata T, Kornberg TB. Hedgehog is a signaling protein with a key role in patterning
770 Drosophila imaginal discs. Cell. 1994;76: 89–102. doi:10.1016/0092-8674(94)90175-9
771 63. O ' Roak BJ, Vives L, Girirajan S, Karakoc E, Krumm N, Coe BP, et al. Sporadic autism
772 exomes reveal a highly interconnected protein network of de novo mutations. Nature.
773 2012;485: 246–250. doi:10.1038/nature10989
774 64. Hahn H, Wicking C, Zaphiropoulos PG, Gailani MR, Shanley S, Chidambaram A, et al.
775 Mutations of the human homolog of drosophila patched in the nevoid basal cell carcinoma
776 syndrome. Cell. 1996;85: 841–851. doi:10.1016/S0092-8674(00)81268-4
777 65. Johnson RL, Rothman AL, Xie J, Goodrich L V., Bare JW, Bonifas JM, et al. Human
778 homolog of patched, a candidate gene for the basal cell nevus syndrome. Science.
779 1996;272: 1668–1671. doi:10.1126/science.272.5268.1668
780 66. Swarup S, Pradhan-Sundd T, Verheyen EM. Genome-wide identification of phospho-
781 regulators of Wnt signaling in Drosophila. Development. 2015;142: 1502–1515.
782 doi:10.1242/dev.116715
783 67. Six EM, Ndiaye D, Sauer G, Laâbi Y, Athman R, Cumano A, et al. The Notch ligand
784 Delta1 recruits Dlg1 at cell-cell contacts and regulates cell migration. J Biol Chem.
785 2004;279: 55818–55826. doi:10.1074/jbc.M408022200
786 68. Greene CS, Krishnan A, Wong AK, Ricciotti E, Zelaya RA, Himmelstein DS, et al.
787 Understanding multicellular function and disease with human tissue-specific networks.
788 Nat Genet. 2015;47: 569–576. doi:10.1038/ng.3259
789 69. Bult CJ, Blake JA, Smith CL, Kadin JA, Richardson JE, Mouse Genome Database Group.
790 Mouse Genome Database (MGD) 2019. Nucleic Acids Res. 2019;47: D801–D806.
791 doi:10.1093/nar/gky1056
792 70. Zhou W, Zhang L, Guoxiang X, Mojsilovic-Petrovic J, Takamaya K, Sattler R, et al.
793 GluR1 controls dendrite growth through its binding partner, SAP97. J Neurosci. 2008;28:
794 10220–10233. doi:10.1523/JNEUROSCI.3434-08.2008
795 71. Iizuka-Kogo A, Ishidao T, Akiyama T, Senda T. Abnormal development of urogenital
796 organs in Dlgh1-deficient mice. Development. 2007;134: 1799–1807.
797 doi:10.1242/dev.02830
798 72. Mahoney ZX, Sammut B, Xavier RJ, Cunningham J, Go G, Brim KL, et al. Discs-large
799 homolog 1 regulates smooth muscle orientation in the mouse ureter. Proc Natl Acad Sci U
800 S A. 2006;103: 19872–19877. doi:10.1073/pnas.0609326103
801 73. Caruana G, Bernstein A. Craniofacial dysmorphogenesis including cleft palate in mice
802 with an insertional mutation in the discs large gene. Mol Cell Biol. 2001;21: 1475–1483.
803 doi:10.1128/MCB.21.5.1475-1483.2001
804 74. Chapman DL, Papaioannou VE. Three neural tubes in mouse embryos with mutations in
805 the T-box gene Tbx6. Nature. 1998;391: 695–697. doi:10.1038/35624
806 75. Ashburner M, Ball CA, Blake JA, Botstein D, Butler H, Cherry JM, et al. Gene ontology:
807 Tool for the unification of biology. Nat. Genet. 2000;25: 25–29. doi:10.1038/75556
808 76. The Gene Ontology Consortium. The Gene Ontology Resource: 20 years and still GOing
809 strong. Nucleic Acids Res. 2019;47: D330–D338. doi:10.1093/nar/gky1055
810 77. Pabis M, Neufeld N, Shav-Tal Y, Neugebauer KM. Binding properties and dynamic

localization of an alternative isoform of the cap-binding complex subunit CBP20. Nucleus. 2010;1: 412–421. doi:10.4161/nucl.1.5.12839

78. Di Padova M, Bruno T, De Nicola F, Iezzi S, D'Angelo C, Gallo R, et al. Che-1 arrests human colon carcinoma cell proliferation by displacing HDAC1 from the p21WAF1/CIP1 promoter. J Biol Chem. 2003;278: 36496–36504. doi:10.1074/jbc.M306694200
79. Bruno T, De Angelis R, De Nicola F, Barbato C, Di Padova M, Corbi N, et al. Che-1 affects cell growth by interfering with the recruitment of HDAC1 by Rb. Cancer Cell. 2002;2: 387–399. doi:10.1016/S1535-6108(02)00182-4
80. Page G, Lödige I, Kögel D, Scheidtmann KH. AATF, a novel transcription factor that interacts with Dlk/ZIP kinase and interferes with apoptosis. FEBS Lett. 1999;462: 187–91. doi:10.1016/s0014-5793(99)01529-x
81. Sumiyoshi E, Sugimoto A, Yamamoto M. Protein phosphatase 4 is required for centrosome maturation in mitosis and sperm meiosis in C. elegans. J Cell Sci. 2002;115: 1403–1410.
82. Jensen M, Girirajan S. An interaction-based model for neuropsychiatric features of copy-number variants. PLoS Genet. 2019;15: e1007879. doi:10.1371/journal.pgen.1007879
83. Girirajan S, Rosenfeld JA, Coe BP, Parikh S, Friedman N, Goldstein A, et al. Phenotypic Heterogeneity of Genomic Disorders and Rare Copy-Number Variants. N Engl J Med. 2012;367: 1321–1331. doi:10.1056/NEJMoa1200395
84. Coe BP, Girirajan S, Eichler EE. A genetic model for neurodevelopmental disease. Curr Opin Neurobiol. 2012;22: 829–836. doi:10.1016/j.conb.2012.04.007
85. Nicholas AK, Swanson EA, Cox JJ, Karbani G, Malik S, Springell K, et al. The molecular landscape of ASPM mutations in primary microcephaly. J Med Genet. 2009;46: 249–253. doi:10.1136/jmg.2008.062380
86. Brand AH, Perrimon N. Targeted gene expression as a means of altering cell fates and generating dominant phenotypes. Development. 1993;118: 401–415. doi:10.1101/lm.1331809
87. Green EW, Fedele G, Giorgini F, Kyriacou CP. A Drosophila RNAi collection is subject to dominant phenotypic effects. Nat Methods. 2014;11: 222–223. doi:10.1038/nmeth.2856
88. Vissers JHA, Manning SA, Kulkarni A, Harvey KF. A Drosophila RNAi library modulates Hippo pathway-dependent tissue growth. Nat Commun. 2016;7: 10368. doi:10.1038/ncomms10368
89. Schindelin J, Arganda-Carreras I, Frise E, Kaynig V, Longair M, Pietzsch T, et al. Fiji: An open-source platform for biological-image analysis. Nat. Methods. 2012;9: 676–682. doi:10.1038/nmeth.2019
90. Kanehisa M, Sato Y, Furumichi M, Morishima K, Tanabe M. New approach for understanding genome variations in KEGG. Nucleic Acids Res. 2019;47: D590–D595. doi:10.1093/nar/gky962
91. Hagberg AA, Schult DA, Swart PJ. Exploring network structure, dynamics, and function using NetworkX. 7th Python in Science Conference (SciPy 2008). 2008. pp. 11–15. Available: http://conference.scipy.org/proceedings/SciPy2008/paper_2
92. Mi H, Huang X, Muruganujan A, Tang H, Mills C, Kang D, et al. PANTHER version 11: Expanded annotation data from Gene Ontology and Reactome pathways, and data analysis tool enhancements. Nucleic Acids Res. 2017;45: D183–D189. doi:10.1093/nar/gkw1138
93. Shannon P, Markiel A, Ozier O, Baliga NS, Wang JT, Ramage D, et al. Cytoscape: A

856 software Environment for integrated models of biomolecular interaction networks.
857 Genome Res. 2003;13: 2498–2504. doi:10.1101/gr.1239303
858

FIGURE LEGENDS

Figure 1. Targeted analysis to identify global developmental phenotypes with knockdown of homologs of CNV genes. (A) Strategy for identifying non-neuronal phenotypes and underlying cellular mechanisms for homologs of CNV and known neurodevelopmental genes using the fly wing as a model system. We evaluated 59 *Drosophila* homologs of genes within 10 CNV regions and 20 known neurodevelopmental genes (79 total homologs). Using the *UAS-GAL4* system with wing-specific bx^{MS1096} driver, we knocked down 136 individual RNAi lines for the CNV and neurodevelopmental homologs, and evaluated qualitative and quantitative phenotypes. We next clustered RNAi lines based on severity of qualitative phenotypes, and compared adult wing phenotypes to phenotypes observed with ubiquitous and eye-specific knockdown of homologs. Furthermore, we evaluated underlying cellular mechanisms for the observed wing-specific phenotypes, and examined the connectivity patterns of candidate homologs for developmental phenotypes in multiple human tissue-specific networks. **(B)** Representative brightfield images of adult wing phenotype severity observed with knockdown of homologs of CNV genes, based on clustering analysis, are shown. **(C)** Heatmap with k-means clustering of qualitative phenotypes in adult female wings across 136 RNAi lines is shown. The color of each cell represents the frequency of individual fly wings (n=20-25 adult wings) for each RNAi line (x-axis) that show a specific severity (no phenotype, mild, moderate, severe, lethal) for the five qualitative phenotypes assessed (y-axis; wrinkled wings, ectopic veins, missing veins, discoloration, bristle planar polarity), as detailed in **Supp. Data 2**. Based on these data, we identified clusters for no phenotype (n=75 lines), mild (n=24 lines), moderate (n=10 lines), severe (n=21 lines), and lethal (n=6 lines). **(D)** Summary table of qualitative and quantitative adult wing phenotypes for all tested RNAi lines of homologs of CNV and

neurodevelopmental genes. Quantitative phenotype totals do not include lethal RNAi lines for both area and vein length. In addition, L3 vein length totals do not include severe RNAi lines.

Figure 2. Qualitative adult wing phenotypes of *Drosophila* homologs of CNV and neurodevelopmental genes. Heatmaps representing the five qualitative adult wing phenotypes for all 136 RNAi lines, with **(A)** all 59 tested homologs for 10 CNV regions and **(B)** 20 homologs for neurodevelopmental genes (β-catenin, core neurodevelopmental genes, and microcephaly genes), are shown. The color of each cell represents the frequency of each of the five qualitative phenotypes by severity (wrinkled wings, WR; ectopic veins, EV; missing veins, MV; discoloration, DC; bristle planar polarity, BP), ranging from no phenotype to lethal. **(C)** Representative brightfield images of adult fly wings (scale bar = 500μm) with wing-specific knockdown of homologs of CNV and neurodevelopmental genes showing the five assessed qualitative phenotypes, including discoloration, wrinkled wings, bristle polarity, ectopic veins, and missing veins are shown. The panels in the bx^{MS1096}*-GAL4* control and $C6836^{KK112485}$ images highlight bristle planar polarity phenotypes for the representative images. Black arrowheads highlight ectopic veins and white arrowheads highlight missing veins. Genotypes for the images are: w^{1118}/bx^{MS1096}*-GAL4;+; UAS-Dicer2/+*, w^{1118}/bx^{MS1096}*-GAL4;UAS-Rph*^{GD7330} *RNAi/+;UAS-Dicer2/+*, w^{1118}/bx^{MS1096}*-GAL4;UAS-CG15528*^{KK107736} *RNAi/+; UAS-Dicer2/+*, w^{1118}/bx^{MS1096}*-GAL4;UAS-CG6836*^{KK112485} *RNAi/+; UAS-Dicer2/+*, w^{1118}/bx^{MS1096}*-GAL4;+;UAS-CG14182*^{GD2738} *RNAi/UAS-Dicer2*, and w^{1118}/bx^{MS1096}*-GAL4;UAS-kis*^{KK100890} *RNAi/+; UAS-Dicer2/+*.

Figure 3. Quantitative adult wing phenotypes of *Drosophila* homologs of CNV and neurodevelopmental genes. (A) Representative brightfield images of adult fly wings (scale bar = 500µm) with wing-specific knockdown of homologs of CNV and neurodevelopmental genes with size defects are shown. The *bx^{MS1096}-GAL4* control image highlights the six veins, including longitudinal veins L2, L3, L4, and L5 as well as the anterior and posterior crossveins (ACV and PCV), that were measured for quantitative analysis. The dotted line in the control image represents the total wing area calculated for each RNAi line. Genotypes for the images are: *w^{1118}/bx^{MS1096}-GAL4;+; UAS-Dicer2/+*, *w^{1118}/bx^{MS1096}-GAL4;UAS-Fmo-2^{KK109203} RNAi/+; UAS-Dicer2/+*, and *w^{1118}/bx^{MS1096}-GAL4;+;UAS-Trpm^{GD4541} RNAi/UAS-Dicer2*. **(B)** Boxplot of L3 vein lengths for knockdown of select homologs in adult fly wings (n = 9-91, *p < 0.05, two-tailed Mann–Whitney test with Benjamini-Hochberg correction). Vein measurements for all other longitudinal veins and crossveins (ACV and PCV) for these lines are represented in **Supp Fig. 2**. **(C)** Boxplot of wing areas for knockdown of select homologs in adult fly wings (n = 9-91, *p < 0.05, two-tailed Mann–Whitney test with Benjamini-Hochberg correction). All boxplots indicate median (center line), 25th and 75th percentiles (bounds of box), and minimum and maximum (whiskers), with red dotted lines representing the control median.

Figure 4. Comparison of wing-specific, eye-specific, and ubiquitous knockdown of homologs of CNV and known neurodevelopmental genes. (A) Heatmap with the penetrance of phenotypes with ubiquitous knockdown (*da–GAL4*) of select homologs of CNV genes, compared to their adult wing-specific (*bx^{MS1096}–GAL4*) phenotypic severity is shown. **(B)** Boxplots of *Flynotyper*-derived phenotypic scores for adult eyes with eye-specific knockdown (*GMR-GAL4*) of select homologs of CNV and neurodevelopmental genes, normalized as fold-

change (FC) to control values (n = 7–40, *p < 0.05, one-tailed Mann–Whitney test with Benjamini-Hochberg correction). The boxplots are arranged by severity of adult wing phenotypes observed for each RNAi line, while the *Flynotyper* phenotypic scores are categorized into four severity categories: no change (0–1.1 FC), mild (1.1–1.5 FC), moderate (1.5–2.0 FC), and severe (>2.0 FC). **(C)** Boxplot showing the average eye phenotypic scores for 66 RNAi lines of select homologs of CNV and neurodevelopmental genes, normalized as fold-change (FC) to control values, by wing phenotypic category (n=4–30 RNAi lines per group). We did not observe any significant changes in eye phenotype severity across the five wing phenotypic categories (Kruskal-Wallis rank sum test, p=0.567, df = 5, $\chi^2 = 3.881$). Examples of average eye phenotypic scores for RNAi lines with no phenotype ($para^{GD3392\_1}$), mild ($rl^{KK115768}$), and lethal ($dlg1^{GD4689}$) wing phenotype severity are highlighted in the graph. All boxplots indicate median (center line), 25th and 75th percentiles (bounds of box), and minimum and maximum (whiskers), with red dotted lines representing the control median. **(D)** Representative brightfield adult eye (scale bar = 100 μm) and adult wing (scale bar = 500μm) images with tissue-specific knockdown of homologs of CNV genes are shown. Genotypes for the eye images are: w^{1118}*;GMR-GAL4/+;* *UAS-Dicer2/+*, w^{1118}*;GMR-GAL4/UAS-Lnk*^{KK105731} *RNAi; UAS-Dicer2/+*, w^{1118}*;GMR-GAL4/UAS-mEFTu1*^{GD16961} *RNAi; UAS-Dicer2/+*. Genotypes for the wing images are: w^{1118}/bx^{MS1096}*-GAL4;+; UAS-Dicer2/+*, w^{1118}/bx^{MS1096}*-GAL4; UAS-Lnk*^{KK105731} *RNAi/+; UAS-Dicer2/+*, and w^{1118}/bx^{MS1096}*-GAL4; UAS-mEFTu1*^{GD16961} *RNAi/+; UAS-Dicer2/+*.

Figure 5. Expression patterns of *Drosophila* homologs and human CNV and neurodevelopmental genes across multiple tissues. (A) Heatmap with expression of fly homologs of select CNV and neurodevelopmental genes in multiple *Drosophila* larval and adult

tissues, derived from the FlyAtlas Anatomical Microarray dataset, compared with adult wing phenotype severity, is shown. Expression values are grouped into no expression (<10 fragments per kilobase of transcript per million reads, or FPKM), low (10–100 FPKM), moderate (100–500 FPKM), high (500–1000 FPKM), and very high (>1000 FPKM) expression categories. **(B)** Heatmap with expression of select human CNV and neurodevelopmental genes in multiple adult tissues, derived from the Genotype-Tissue Expression (GTEx) dataset v.1.2, is shown. Expression values are grouped into no expression (<3 transcripts per million reads, or TPM), low (3–10 TPM), moderate (10–25 TPM), high (25–100 TPM), and very high (>100 TPM) expression categories. X symbols denote preferential expression in a particular tissue (see Methods). Expression data for all CNV and neurodevelopmental genes are provided in **Supp. Data 6**.

Figure 6. *Drosophila* homologs of CNV and neurodevelopmental genes show altered levels of apoptosis and proliferation. (A) Larval imaginal wing discs (scale bar = 50 μm) stained with nuclear marker DAPI, apoptosis marker dcp1, and cell proliferation marker pH3 illustrate altered levels of apoptosis and cell proliferation due to wing-specific knockdown of select fly homologs of CNV genes. We quantified the number of stained cells within the wing pouch of the wing disc (white box), which becomes the adult wing. Additional representative images of select homologs are presented in **Supp Fig. 5**. Genotypes for the wing images are: w^{1118}/bx^{MS1096}*-GAL4;+; UAS-Dicer2/+*, w^{1118}/bx^{MS1096}*-GAL4;+; UAS-Aatf*^{GD7229} *RNAi/UAS-Dicer2*, w^{1118}/bx^{MS1096}*-GAL4;UAS-Pp4-19C*^{GD9561}*/+; UAS-Dicer2/+*, w^{1118}/bx^{MS1096}*-GAL4;+; UAS-Atx2*^{GD11562} *RNAi/UAS-Dicer2*, and w^{1118}/bx^{MS1096}*-GAL4;+; UAS-Sin*^{GD7027} *RNAi/UAS-Dicer2*. **(B)** Box plot of dcp1-positive cells in larval wing discs with knockdown of select fly homologs of CNV and

neurodevelopmental genes, normalized to controls (n = 7–18, *p < 0.05, two-tailed Mann–Whitney test with Benjamini-Hochberg correction). We note that several RNAi lines showed severe dcp1 staining across the entire wing disc and could not be quantified. The number of dcp1 positive cells were calculated manually. **(C)** Box plot of pH3-positive cells in the larval wing discs with knockdown of select fly homologs of CNV and neurodevelopmental genes, normalized to controls (n = 6–18, *p < 0.05, two-tailed Mann–Whitney test with Benjamini-Hochberg correction). The number of pH3 positive cells were calculated using the AnalyzeParticles function in ImageJ. All boxplots indicate median (center line), 25th and 75th percentiles (bounds of box), and minimum and maximum (whiskers), with red dotted lines representing the control median.

Figure 7. Candidate *Drosophila* homologs of genes within CNV regions interact with conserved signaling pathways. Larval imaginal wing discs (scale bar = 50 μm) stained with **(A)** wingless, **(B)** patched, **(C)** engrailed, and **(D)** delta illustrate disrupted expression patterns for proteins located within the Wnt (wingless), Hedgehog (patched and engrailed), and Notch (delta) signaling pathways due to wing-specific knockdown of select fly homologs of CNV and neurodevelopmental genes. Dotted yellow boxes represent expected expression patterns for signaling proteins in bx^{MS1096}-*GAL4* control images. White arrowheads and dotted white boxes highlight disruptions in expression patterns of signaling proteins with knockdown of CNV or neurodevelopmental genes. Additional representative images of select homologs are presented in **Supp Fig. 7**. Genotypes for the wing images are: w^{1118}/bx^{MS1096}-*GAL4;+; UAS-Dicer2/+*, w^{1118}/bx^{MS1096}-*GAL4;UAS-Pp4-19C*^{GD9561}*/+; UAS-Dicer2/+*, w^{1118}/bx^{MS1096}-*GAL4;UAS-Cbp20*^{KK109448}*/+; UAS-Dicer2/+*, w^{1118}/bx^{MS1096}-*GAL4;+; UAS-Sin*^{GD7027} *RNAi/UAS-Dicer2,*

996 *w^{1118}/bx^{MS1096}-GAL4;+; UAS-Aatf^{GD7229} RNAi/UAS-Dicer2*, and *w^{1118}/bx^{MS1096}-GAL4;UAS-*

997 *Klp61F^{GD14149}/+; UAS-Dicer2/+*.

998

999 **Figure 8. Connectivity of human CNV genes with conserved signaling pathway genes in**

1000 **human tissue-specific networks. (A)** Representative diagrams of eight human CNV and

1001 neurodevelopmental genes whose fly homologs disrupt the Notch signaling pathway and 57

1002 human Notch signaling genes within kidney, heart, and brain-specific gene interaction networks

1003 are shown. Yellow nodes represent CNV and neurodevelopmental genes, pink nodes represent

1004 Notch signaling pathway genes, and green nodes represent connector genes within the shortest

1005 paths between CNV and Notch pathway genes. **(B)** Violin plots showing the average

1006 connectivity (i.e. inverse of shortest path lengths) of CNV genes to genes in Hedgehog, Notch,

1007 and Wnt signaling pathways across the tested tissue-specific networks (n=322–810 pairwise

1008 interactions, *$p < 0.05$, two-tailed Welch's t-test with Benjamini-Hochberg correction). **(C)**

1009 Table showing enriched clusters of Gene Ontology (GO) Biological Process terms for connector

1010 genes observed for each signaling pathway in the three tested tissue-specific networks,

1011 categorized by enrichments in ubiquitous, neuronal, and non-neuronal tissues ($p<0.05$, Fisher's

1012 Exact test with Benjamini-Hochberg correction).

1013

1014 **Figure 9. A multigenic model for neuronal and non-neuronal phenotypes associated with**

1015 **pathogenic CNVs.** Schematic of a multigenic model for neuronal and non-neuronal phenotypes

1016 associated with pathogenic CNVs. While a subset of genes within CNV regions contribute

1017 towards tissue-specific phenotypes, a majority of genes contribute towards both neuronal and

1018 non-neuronal phenotypes through disruption of developmental signaling pathways and global

1019 biological processes.

SUPPLEMENTARY LEGENDS

Supplementary Figure 1. Quantitative vein length phenotypes for select *Drosophila* homologs of CNV and neurodevelopmental genes. Boxplots of longitudinal veins **(A)** L2, **(B)** L4, **(C)** L5, and **(D)** anterior crossvein (ACV) and **(E)** posterior crossvein (PCV) lengths for knockdown of select homologs in adult fly wings (n = 9-91, *p < 0.05, two-tailed Mann–Whitney test with Benjamini-Hochberg correction). All boxplots indicate median (center line), 25th and 75th percentiles (bounds of box), and minimum and maximum (whiskers), with red dotted lines representing the control median.

Supplementary Figure 2. Comparisons of eye-specific and wing-specific knockdowns for select *Drosophila* homologs of CNV and neurodevelopmental genes. Boxplots of *Flynotyper*-derived phenotypic scores for 66 tested adult eyes with eye-specific knockdown (*GMR-GAL4*) of select homologs of CNV and neurodevelopmental genes, normalized as fold-change (FC) to control values (n = 1–40, *p < 0.05, one-tailed Mann–Whitney test with Benjamini-Hochberg correction). RNAi lines that do not show any observable qualitative adult wing phenotypes, including lines that show wing measurement phenotypes, are represented in **(A)**, and RNAi lines with observable mild to lethal qualitative wing phenotypes are represented in **(B)**. All boxplots indicate median (center line), 25th and 75th percentiles (bounds of box), and minimum and maximum (whiskers), with red dotted lines representing the control median.

Supplementary Figure 3. Expression of *Drosophila* homologs of CNV and neurodevelopmental genes in larval and adult tissues. Venn diagrams representing the number of 76/77 tested fly homologs for CNV and neurodevelopmental genes expressed (>10

fragments per kilobase of transcript per million reads, or FPKM) in **(A)** larval (central nervous system or CNS, gut, trachea, and fat body) and **(B)** adult tissues (brain, gut, heart and fat body), are shown.

Supplementary Figure 4. Additional *Drosophila* homologs of CNV and neurodevelopmental genes show altered levels of cell proliferation and apoptosis. Larval imaginal wing discs (scale bar = 50 μm) stained with nuclear marker DAPI, apoptosis marker dcp1, and cell proliferation marker pH3 illustrate altered levels of cell proliferation and apoptosis due to wing-specific knockdown of select fly homologs of CNV genes. We examined changes in the number of stained cells within the wing pouch of the wing disc (white box), which becomes the adult wing. Genotypes for the wing images are: w^{1118}/bx^{MS1096}-*GAL4;+; UAS-Dicer2/+*, w^{1118}/bx^{MS1096}-*GAL4;UAS-Cbp20*^{KK109448}*/+; UAS-Dicer2/+*, w^{1118}/bx^{MS1096}-*GAL4;+; UAS-dlg1*^{GD4689} *RNAi/UAS-Dicer2*, w^{1118}/bx^{MS1096}-*GAL4;UAS-CG8888*^{GD3777}*/+; UAS-Dicer2/+*, w^{1118}/bx^{MS1096}-*GAL4;+; UAS-UQCR-C2*^{GD11238} *RNAi/UAS-Dicer2*, w^{1118}/bx^{MS1096}-*GAL4;+; UAS-ACC*^{GD3482} *RNAi/UAS-Dicer2*, w^{1118}/bx^{MS1096}-*GAL4;UAS-Klp61F*^{GD14149}*/+; UAS-Dicer2/+*, and w^{1118}/bx^{MS1096}-*GAL4;UAS-Rph*^{GD7330} *RNAi/+;UAS-Dicer2/+*.

Supplementary Figure 5. Select female and male *Drosophila* homologs of CNV and neurodevelopmental genes show altered levels of cell proliferation and apoptosis. (A) Larval imaginal wing discs (scale bar = 50 μm) stained with nuclear marker DAPI, apoptosis marker dcp1, and cell proliferation marker pH3 illustrate altered levels of cell proliferation and apoptosis due to wing-specific knockdown of select fly homologs of CNV genes in females and males. We examined changes in the number of stained cells within the wing pouch of the wing disc (white

box), which becomes the adult wing. Genotypes for the wing images are: w^{1118}/bx^{MS1096}-*GAL4;+; UAS-Dicer2/+*, w^{1118}/bx^{MS1096}-*GAL4;+; UAS-lgs*^{GD1241}*/UAS-Dicer2*, w^{1118}/bx^{MS1096}-*GAL4;+; UAS-Sra-1*^{GD11477}*/UAS-Dicer2*, and w^{1118}/bx^{MS1096}-*GAL4;UAS-CG11035*^{KK101201} *RNAi+; UAS-Dicer2/+*. **(B)** Box plot of dcp1-positive cells in larval wing discs with knockdown of select fly homologs of CNV and neurodevelopmental genes, normalized to controls ($n = 9–13$, $*p < 0.05$, two-tailed Mann–Whitney test with Benjamini-Hochberg correction). The number of dcp1 positive cells were calculated manually. **(C)** Box plot of pH3-positive cells in the larval wing discs with knockdown of select fly homologs of CNV and neurodevelopmental genes, normalized to controls ($n = 9–13$, $*p < 0.05$, two-tailed Mann–Whitney test with Benjamini-Hochberg correction). The number of pH3 positive cells were calculated using the AnalyzeParticles function in ImageJ. All boxplots indicate median (center line), 25th and 75th percentiles (bounds of box), and minimum and maximum (whiskers), with red dotted lines representing the control median.

Supplementary Figure 6. Additional *Drosophila* homologs of genes within CNV regions interact with conserved signaling pathways to induce developmental phenotypes. Larval imaginal wing discs (scale bar = 50 μm) stained with **(A)** wingless, **(B)** patched, **(C)** engrailed, and **(D)** delta illustrate disrupted expression patterns for proteins located within the Wnt (wingless), Hedgehog (patched and engrailed), and Notch (delta) signaling pathways due to wing-specific knockdown of additional fly homologs of CNV and neurodevelopmental genes. Dotted yellow boxes represent expected expression patterns for signaling proteins in bx^{MS1096}-*GAL4* control images. White arrowheads and dotted white boxes highlight disruptions in expression patterns of signaling proteins with knockdown of CNV or neurodevelopmental genes.

Genotypes for the wing images are: *w*^{1118}/*bx*^{MS1096}-*GAL4;+; UAS-Dicer2/+*, *w*^{1118}/*bx*^{MS1096}-*GAL4;+; UAS-dlg1*^{GD4689} *RNAi/UAS-Dicer2*, *w*^{1118}/*bx*^{MS1096}-*GAL4;+; UAS-Tsf2*^{GD2442} *RNAi/UAS-Dicer2*, *w*^{1118}/*bx*^{MS1096}-*GAL4;+; UAS-Atx2*^{GD11562} *RNAi/UAS-Dicer2*, *w*^{1118}/*bx*^{MS1096}-*GAL4;+; UAS-UQCR-C2*^{GD11238} *RNAi/UAS-Dicer2*, *w*^{1118}/*bx*^{MS1096}-*GAL4;+; UAS-nudE*^{GD15226} *RNAi/UAS-Dicer2*, and *w*^{1118}/*bx*^{MS1096}-*GAL4;+; UAS-ACC*^{GD3482} *RNAi/UAS-Dicer2*.

Supplementary Figure 7. Tissue-specific network diagrams showing connectivity of human CNV genes with conserved signaling pathway genes. Representative network diagrams of nine human CNV and neurodevelopmental genes whose fly homologs disrupt the **(A)** Wnt and **(B)** Hedgehog signaling pathway and 162 human Wnt and 46 human Hedgehog signaling genes within kidney, heart, and brain-specific gene interaction networks are shown. Yellow nodes represent CNV and neurodevelopmental genes, pink nodes represent Notch signaling pathway genes, and green nodes represent connector genes within the shortest paths between CNV and Notch pathway genes.

Supplementary Data 1 (Excel file). *Drosophila* homologs of human CNV and neurodevelopmental genes as determined using DIOPT v.7.1.

Supplementary Data 2 (Excel file). Qualitative and quantitative adult wing phenotypic data for *Drosophila* homologs of human CNV and neurodevelopmental genes. This file shows the raw frequencies of severity for the five qualitative wing phenotypes and average areas and vein lengths for all 136 female and male tested RNAi lines. In addition, this file also includes k-means clustering analysis for the female RNAi lines.

Supplementary Data 3 (Excel file). Summary of adult wing qualitative and quantitative phenotypes by *Drosophila* homologs. This file summarizes qualitative k-means clustering and longitudinal L3 vein length and wing area changes for all 136 RNAi lines by fly homologs. We define discordant homologs when RNAi lines for the same homologs showed inconsistent wing phenotypes. For each homolog with multiple RNAi lines, we checked discordance among RNAi lines for no phenotype versus any qualitative or quantitative phenotypes, followed by discordance for small or large quantitative phenotypes.

Supplementary Data 4 (Excel file). Phenotypes of mouse knockdown models for homologs of CNV genes. This file lists lethality and neuronal and non-neuronal phenotypes, categorized using top-level Mammalian Phenotype Ontology terms, for knockdown models of 130 mouse homologs of CNV genes derived from the Mouse Genome Informatics (MGI) database.

Supplementary Data 5 (Excel file). Summary of eye-specific and wing-specific phenotypes for fly homologs. This file summarizes eye-specific and wing-specific phenotypes by severity category for 66 RNAi lines by fly homologs of CNV and neurodevelopmental genes. Eye phenotype severity is defined by *Flynotyper* phenotypic scores with fold-change (FC) normalization to control as follows: no change (0–1.1 FC), mild (1.1–1.5 FC), moderate (1.5–2.0 FC), and severe (>2.0 FC). Wing phenotype severity is defined by k-means clustering for qualitative phenotypes and quantitative size changes as listed in **Supp. Data 3**.

Supplementary Data 6 (Excel file). Tissue-specific expression of *Drosophila* homologs and human CNV and neurodevelopmental genes. This file lists expression values across multiple fly and human tissues for all 79 *Drosophila* homologs and 150 human genes. Fly expression data (fragments per kilobase of transcript per million reads, or FPKM) was derived from the FlyAtlas Anatomical Microarray dataset, and human expression data (transcripts per million reads, or TPM) was derived from the Genotype-Tissue Expression (GTEx) dataset v.1.2.

Supplementary Data 7 (Excel file). Summary of immunostaining of the larval imaginal wing discs. This file summarizes changes in apoptosis (27 homologs), cell proliferation (27 homologs), and Wnt, Hedgehog, and Notch signaling pathway proteins (14 homologs), along with qualitative and quantitative adult wing phenotypes (as listed in **Supp. Data 2.**), for female and male fly homologs.

Supplementary Data 8 (Excel file). Tissue-specific network connectivity for candidate CNV genes and signaling pathway genes. This file lists the shortest path lengths between nine candidate CNV genes and 265 genes within Wnt, Hedgehog, and Notch signaling pathways for heart, kidney, and brain-specific gene interaction networks, along with the connector genes that are within the shortest paths. Enriched Gene Ontology (GO) Biological Process, Cellular Component, and Molecular Function terms for sets of connector genes for each signaling pathway in each tissue-specific networks are also represented.

Supplementary Data 9 (Excel file). List of *Drosophila* stocks used for experiments, including stock numbers and genotypes.

Supplementary Data 10 (Excel file). Statistics for all experimental data. This file shows all statistical information (sample size, mean/median/standard deviation of datasets, test statistics, p-values, degrees of freedom, confidence intervals, and Benjamini-Hochberg FDR corrections) for all data. Statistical information for Kruskal-Wallis test includes factors, degrees of freedom, test statistics, and post-hoc pairwise Wilcoxon tests with Benjamini-Hochberg correction.

Figure 1

A Experimental strategy

Wing-specific driver *bx^{MS1096}-GAL4* × ***UAS-RNAi*** (79 genes)

Phenotyping of adult wings

Qualitative analysis
- Wrinkled wings
- Ectopic veins
- Missing veins
- Discoloration
- Bristle planar polarity

Quantitative analysis
- Longitudinal veins (L2,L3,L4,L5)
- Crossveins (ACV, PCV)
- Wing area

Tissue-specific effects
- Compare to ubiquitous knockdown
- Compare to eye-specific knockdown
- Gene expression across multiple tissues (Human and flies)

Cellular processes and developmental pathways
- Apoptosis
- Cell proliferation
- Disruptions in signaling pathways
- Human tissue-specific network analysis (Brain, heart, kidney)

B Phenotypic analysis of adult wings in *Drosophila*

C K-means clustering of qualitative wing data

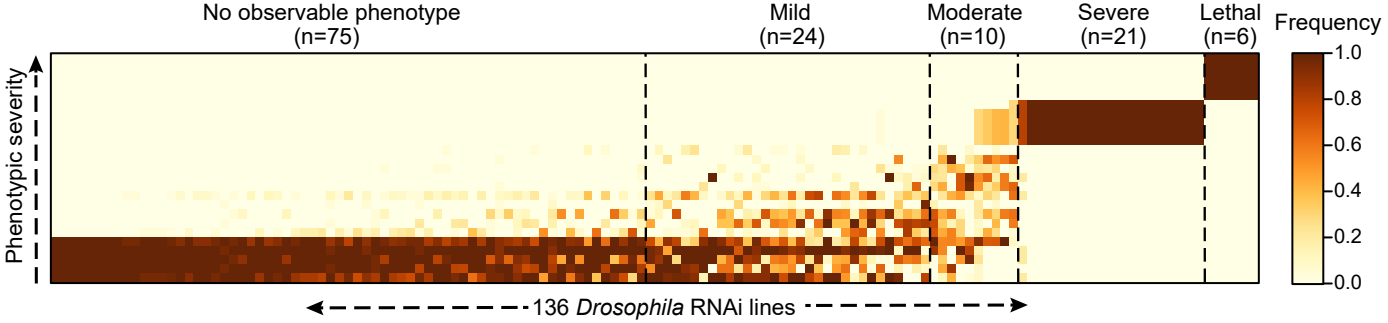

D Summary of qualitative and quantitative adult wing phenotypes

Fly homologs	RNAi lines	Qualitative phenotypes					Quantitative phenotypes	
		No pheno.	Mild	Moderate	Severe	Lethal	Wing area	L3 vein length
CNV genes (15q11.2, 15q13.3, 16p11.2, Distal 16p11.2, 16p12.1, 16p13.11, 17q12, 1q21.1, 3q29, 7q11.23)	95	45	21	7	16	6	65	53
Known neurodevelopmental genes (β-catenin, core genes, microcephaly)	41	30	3	3	5	0	24	21
Total	136	75	24	10	21	6	89	74

Figure 2

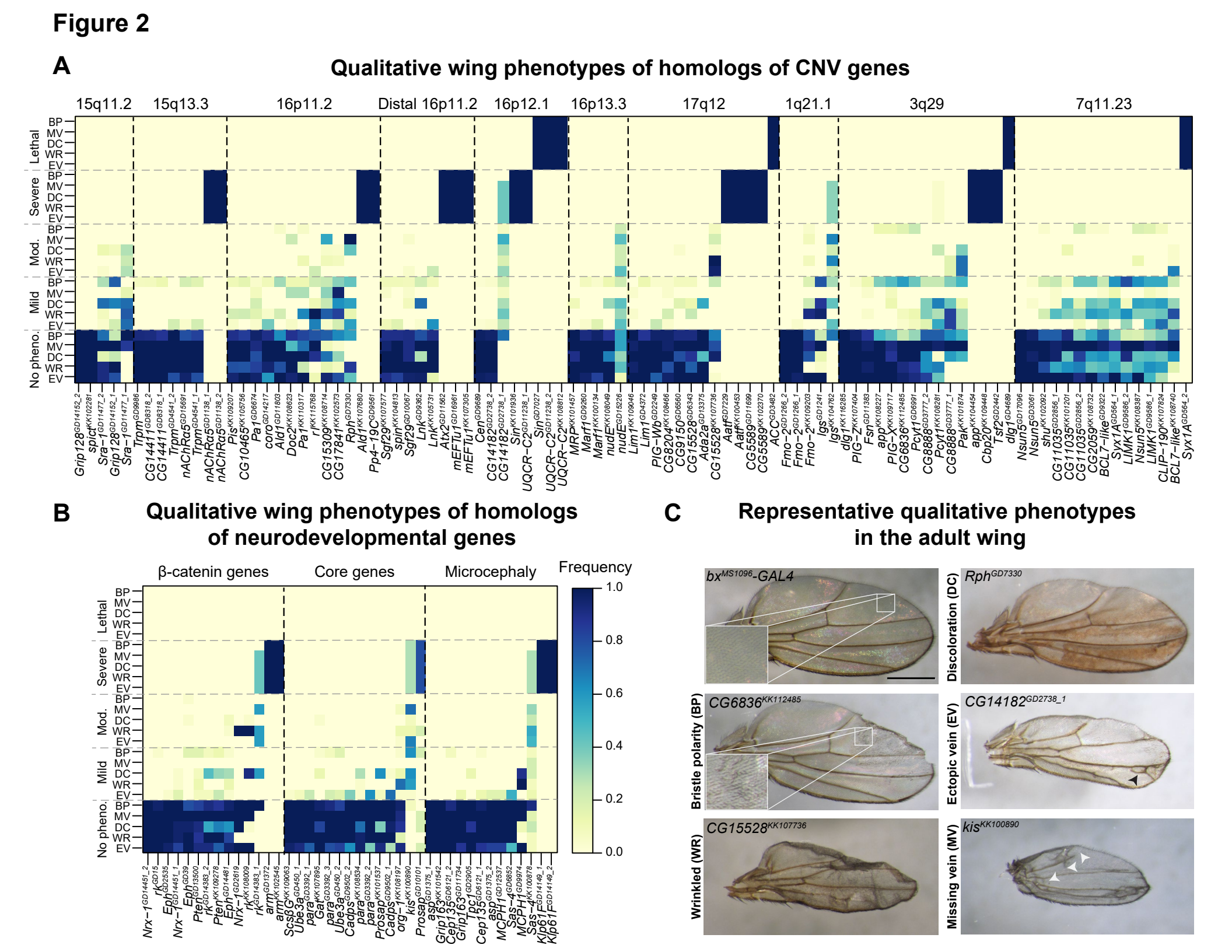
A
Qualitative wing phenotypes of homologs of CNV genes
15q11.2
15q13.3
16p11.2
Distal 16p11.2
16p12.1
16p13.3
17q12
1q21.1
3q29
7q11.23
Lethal
Severe
Mod.
Mild
No pheno.
BP
MV
DC
WR
EV
B
Qualitative wing phenotypes of homologs of neurodevelopmental genes
β-catenin genes
Core genes
Microcephaly
Frequency
1.0
0.8
0.6
0.4
0.2
0.0
C
Representative qualitative phenotypes in the adult wing
bx^MS1096-GAL4
Rph^GD7330
Discoloration (DC)
CG6836^KK112485
Bristle polarity (BP)
CG14182^GD2738_1
Ectopic vein (EV)
CG15528^KK107736
Wrinkled (WR)
kis^KK100890
Missing vein (MV)

Figure 3

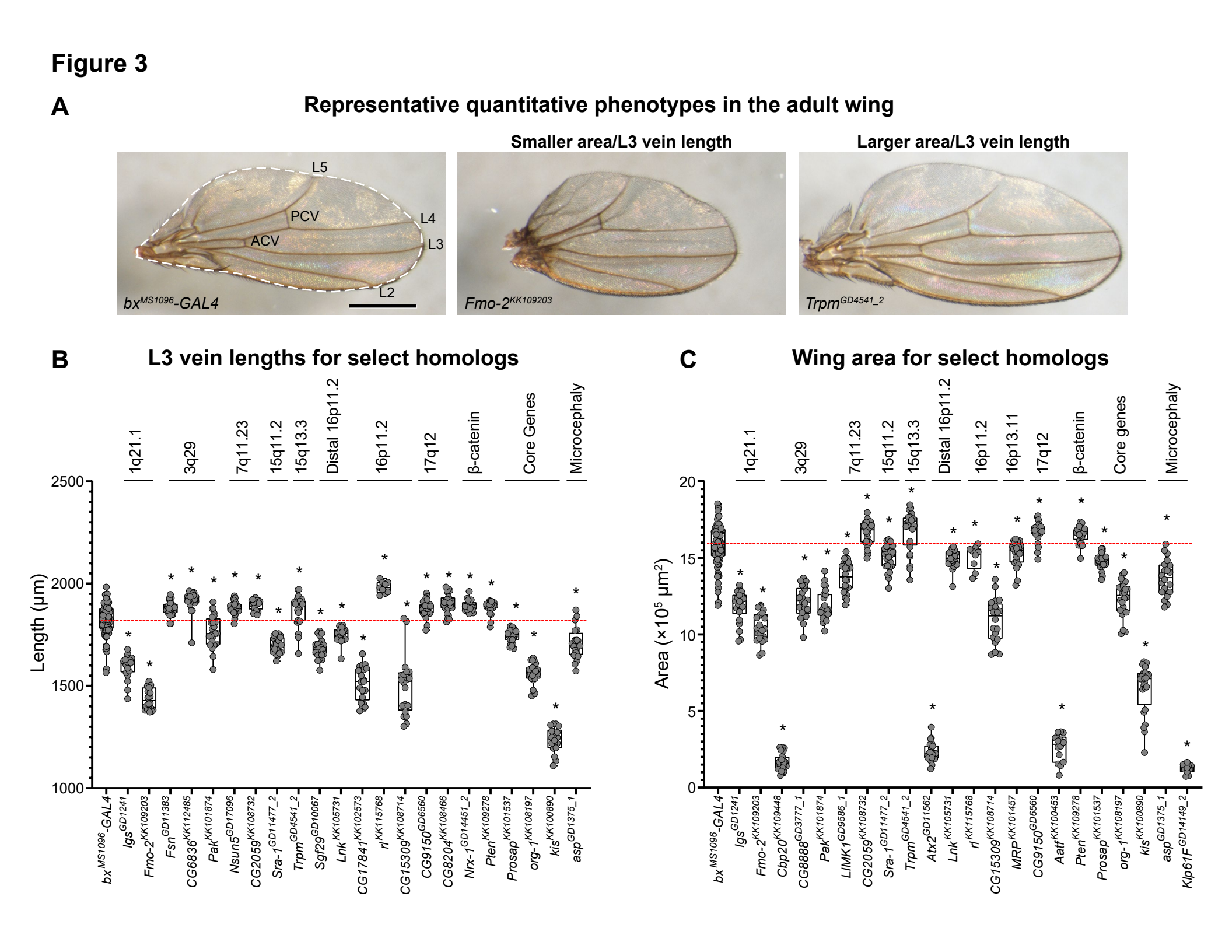
A
Representative quantitative phenotypes in the adult wing
Smaller area/L3 vein length
Larger area/L3 vein length
L5
PCV
ACV
L4
L3
L2
bx^MS1096-GAL4
Fmo-2^KK109203
Trpm^GD4541_2
B
L3 vein lengths for select homologs
C
Wing area for select homologs
1q21.1
3q29
7q11.23
15q11.2
15q13.3
Distal 16p11.2
16p11.2
17q12
β-catenin
Core Genes
Microcephaly
16p13.11
Core genes
Length (µm)
Area (×10^5 µm^2)
bx^MS1096-GAL4
lgs^GD1241
Fmo-2^KK109203
Fsn^GD11383
CG6836^KK112485
Pak^KK101874
Nsun5^GD17096
CG2059^KK108732
Sra-1^GD11477_2
Trpm^GD4541_2
Sgf29^GD10067
Lnk^KK105731
CG17841^KK102573
rl^KK115768
CG15309^KK108714
CG9150^GD6560
CG8204^KK108466
Nrx-1^GD14451_2
Pten^KK109278
Prosap^KK101537
org-1^KK108197
kis^KK100890
asp^GD1375_1
Cbp20^KK109448
CG8888^GD3777_1
LIMK1^GD9586_1
Atx2^GD11562
MRP^KK101457
Aatf^KK100453
Klp61F^GD14149_2

Figure 4

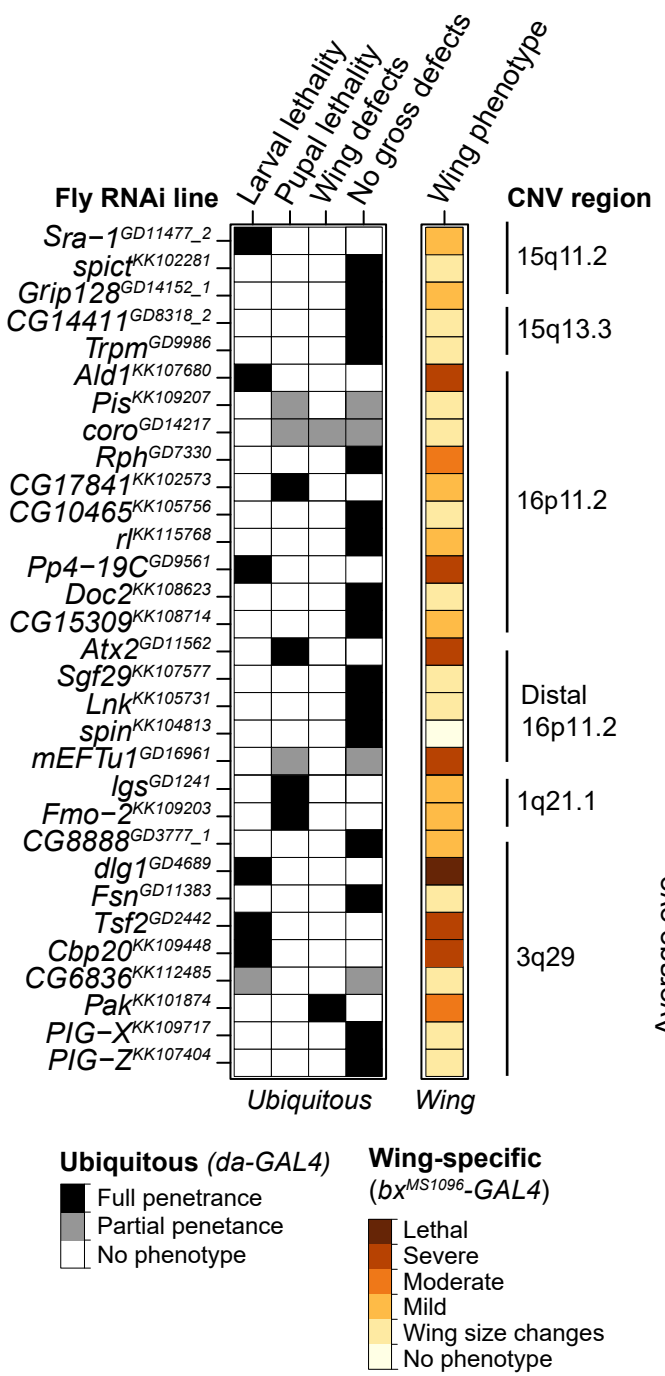
A
Ubiquitous knockdown
Larval lethality
Pupal lethality
Wing defects
No gross defects
Wing phenotype
Fly RNAi line
CNV region
Sra−1GD11477_2
spictKK102281
Grip128GD14152_1
CG14411GD8318_2
TrpmGD9986
Ald1KK107680
PisKK109207
coroGD14217
RphGD7330
CG17841KK102573
CG10465KK105756
rlKK115768
Pp4−19CGD9561
Doc2KK108623
CG15309KK108714
Atx2GD11562
Sgf29KK107577
LnkKK105731
spinKK104813
mEFTu1GD16961
lgsGD1241
Fmo−2KK109203
CG8888GD3777_1
dlg1GD4689
FsnGD11383
Tsf2GD2442
Cbp20KK109448
CG6836KK112485
PakKK101874
PIG−XKK109717
PIG−ZKK107404
15q11.2
15q13.3
16p11.2
Distal 16p11.2
1q21.1
3q29
Ubiquitous
Wing
Ubiquitous (da-GAL4)
Full penetrance
Partial penetance
No phenotype
Wing-specific (bxMS1096-GAL4)
Lethal
Severe
Moderate
Mild
Wing size changes
No phenotype

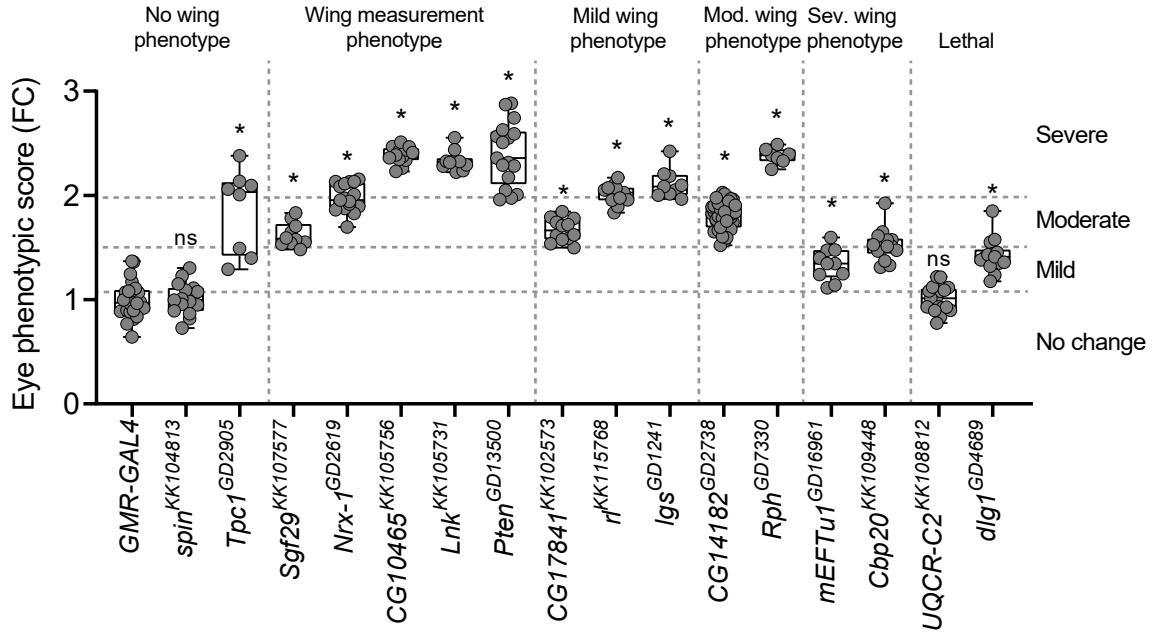
B
Eye versus wing phenotypes
No wing phenotype
Wing measurement phenotype
Mild wing phenotype
Mod. wing phenotype
Sev. wing phenotype
Lethal
Eye phenotypic score (FC)
Severe
Moderate
Mild
No change
ns
GMR-GAL4
spinKK104813
Tpc1GD2905
Sgf29KK107577
Nrx-1GD2619
CG10465KK105756
LnkKK105731
PtenGD13500
CG17841KK102573
rlKK115768
lgsGD1241
CG14182GD2738
RphGD7330
mEFTu1GD16961
Cbp20KK109448
UQCR-C2KK108812
dlg1GD4689

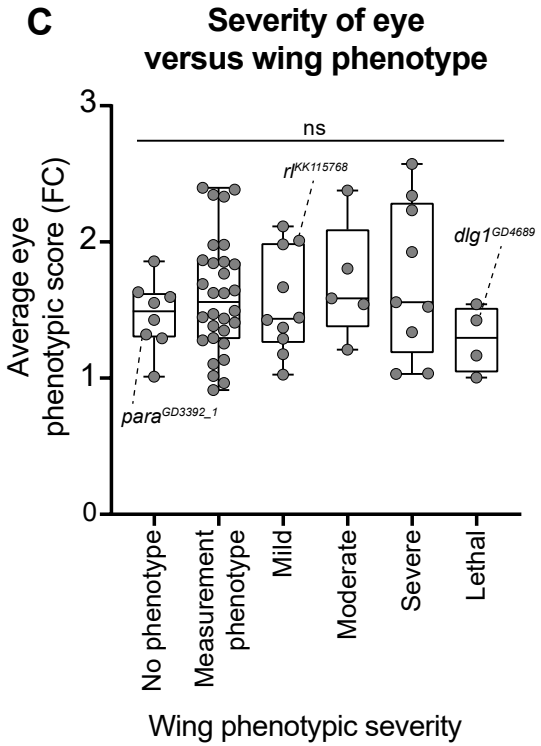
C
Severity of eye versus wing phenotype
Average eye phenotypic score (FC)
ns
rlKK115768
dlg1GD4689
paraGD3392_1
No phenotype
Measurement phenotype
Mild
Moderate
Severe
Lethal
Wing phenotypic severity

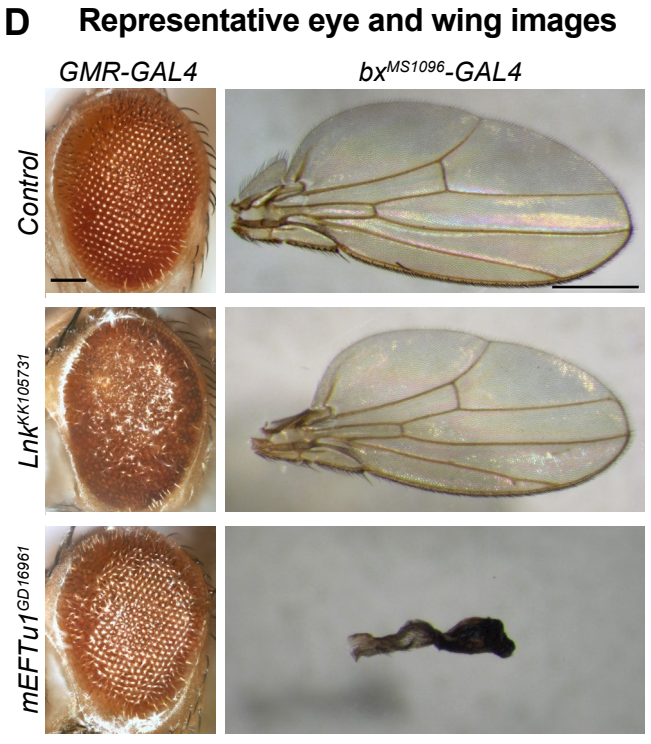
D
Representative eye and wing images
GMR-GAL4
bxMS1096-GAL4
Control
LnkKK105731
mEFTu1GD16961

Figure 5

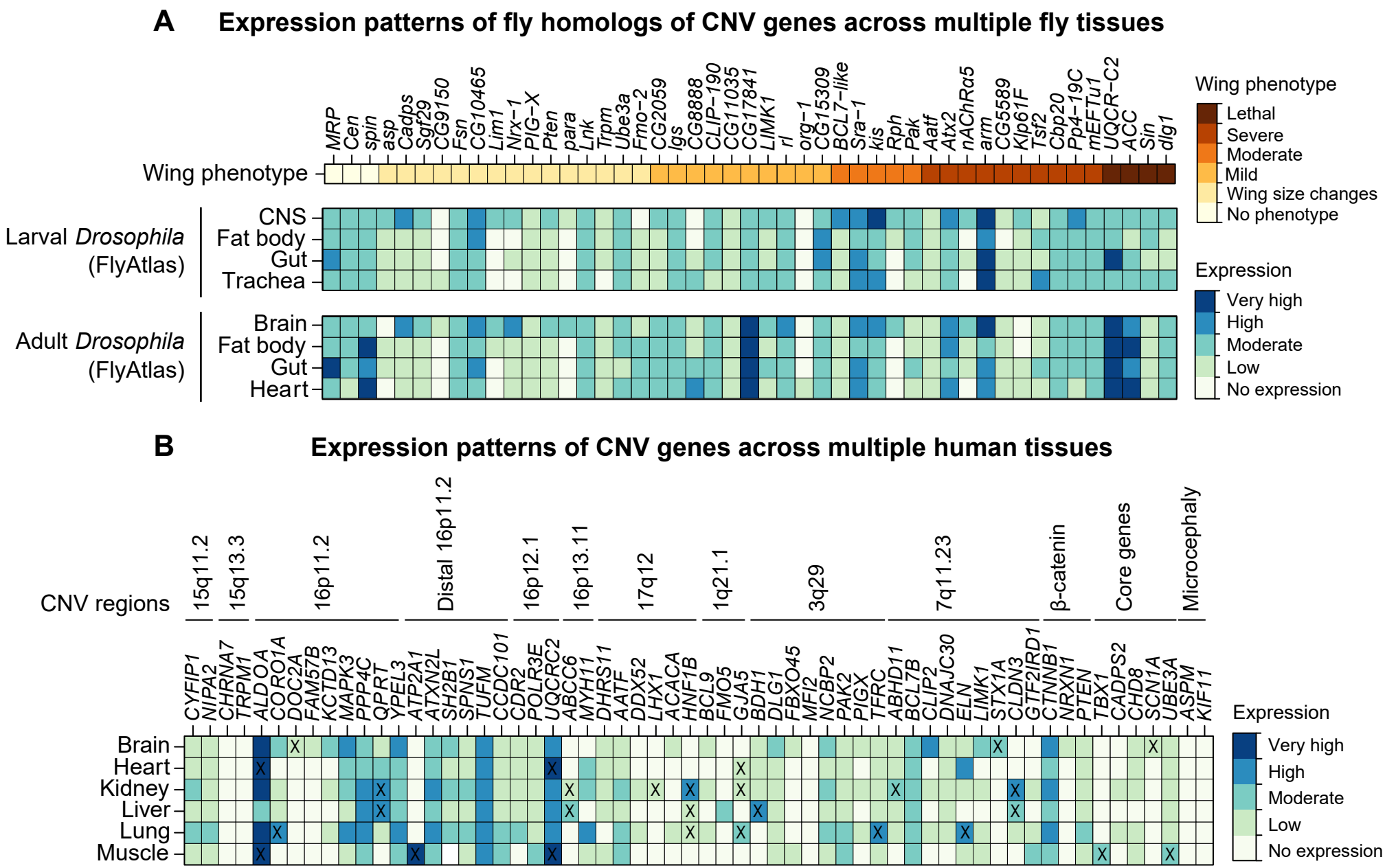
A
Expression patterns of fly homologs of CNV genes across multiple fly tissues
MRP Cen spin asp Cadps Sgf29 CG9150 Fsn CG10465 Lim1 Nrx−1 PIG−X Pten para Lnk Trpm Ube3a Fmo−2 CG2059 Igs CG8888 CLIP−190 CG11035 CG17841 LIMK1 rl org−1 CG15309 BCL7−like Sra−1 kis Rph Pak Aatf Atx2 nAChRα5 arm CG5589 Klp61F Tsf2 Cbp20 Pp4−19C mEFTu1 UQCR−C2 ACC Sin dlg1
Wing phenotype
Larval Drosophila (FlyAtlas)
CNS
Fat body
Gut
Trachea
Adult Drosophila (FlyAtlas)
Brain
Fat body
Gut
Heart
Wing phenotype
Lethal
Severe
Moderate
Mild
Wing size changes
No phenotype
Expression
Very high
High
Moderate
Low
No expression
B
Expression patterns of CNV genes across multiple human tissues
CNV regions
15q11.2
15q13.3
16p11.2
Distal 16p11.2
16p12.1
16p13.11
17q12
1q21.1
3q29
7q11.23
β-catenin
Core genes
Microcephaly
CYFIP1 NIPA2 CHRNA7 TRPM1 ALDOA CORO1A DOC2A FAM57B KCTD13 MAPK3 PPP4C QPRT YPEL3 ATP2A1 ATXN2L SH2B1 SPNS1 TUFM CCDC101 CDR2 POLR3E UQCRC2 ABCC6 MYH11 DHRS11 AATF DDX52 LHX1 ACACA HNF1B BCL9 FMO5 GJA5 BDH1 DLG1 FBXO45 MFI2 NCBP2 PAK2 PIGX TFRC ABHD11 BCL7B CLIP2 DNAJC30 ELN LIMK1 STX1A CLDN3 GTF2IRD1 CTNNB1 NRXN1 PTEN TBX1 CADPS2 CHD8 SCN1A UBE3A ASPM KIF11
Brain
Heart
Kidney
Liver
Lung
Muscle
Expression
Very high
High
Moderate
Low
No expression

Figure 6

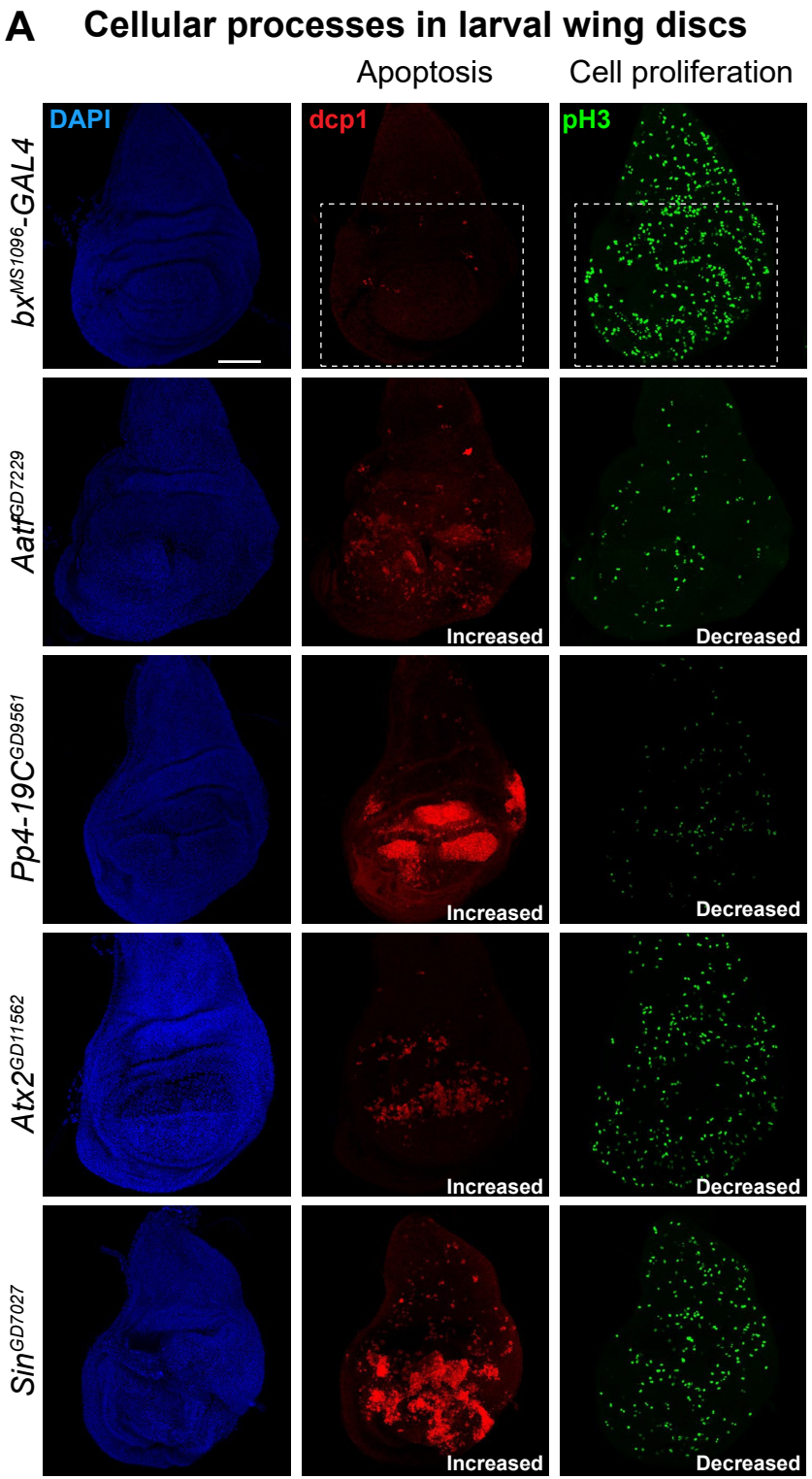
A
Cellular processes in larval wing discs
Apoptosis
Cell proliferation
DAPI
dcp1
pH3
bx^MS1096-GAL4
Aatf^GD7229
Pp4-19C^GD9561
Atx2^GD11562
Sin^GD7027
Increased
Decreased

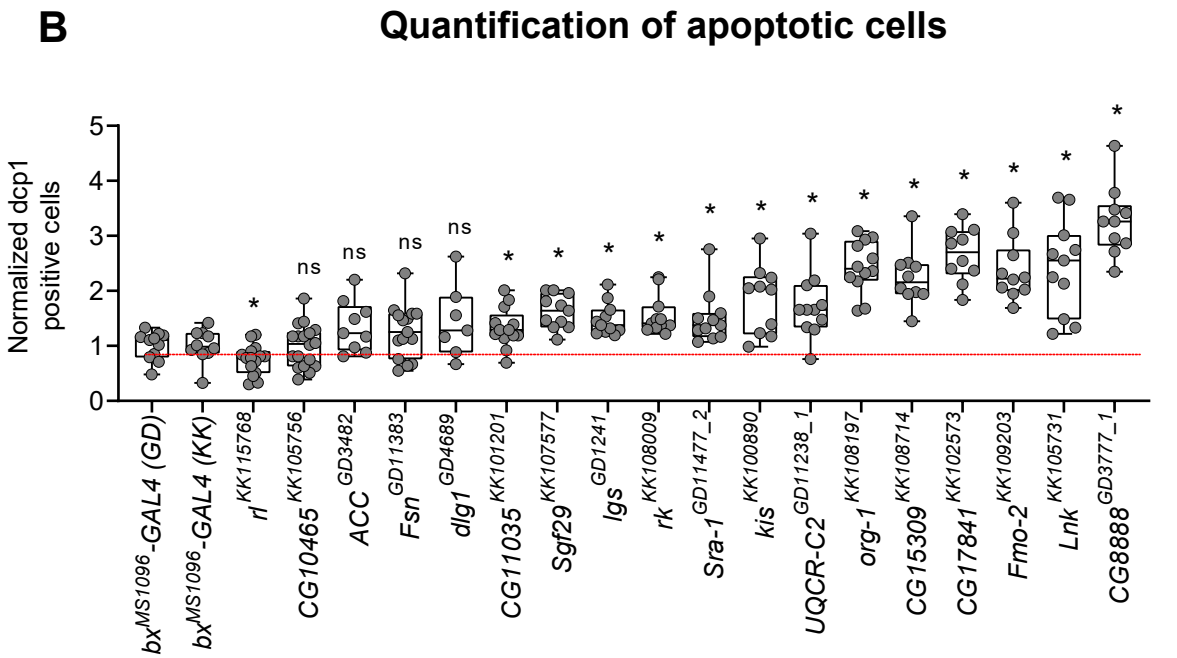
B
Quantification of apoptotic cells
Normalized dcp1 positive cells
bx^MS1096-GAL4 (GD)
bx^MS1096-GAL4 (KK)
rl^KK115768
CG10465^KK105756
ACC^GD3482
Fsn^GD11383
dlg1^GD4689
CG11035^KK101201
Sgf29^KK107577
lgs^GD1241
rk^KK108009
Sra-1^GD11477_2
kis^KK100890
UQCR-C2^GD11238_1
org-1^KK108197
CG15309^KK108714
CG17841^KK102573
Fmo-2^KK109203
Lnk^KK105731
CG8888^GD3777_1

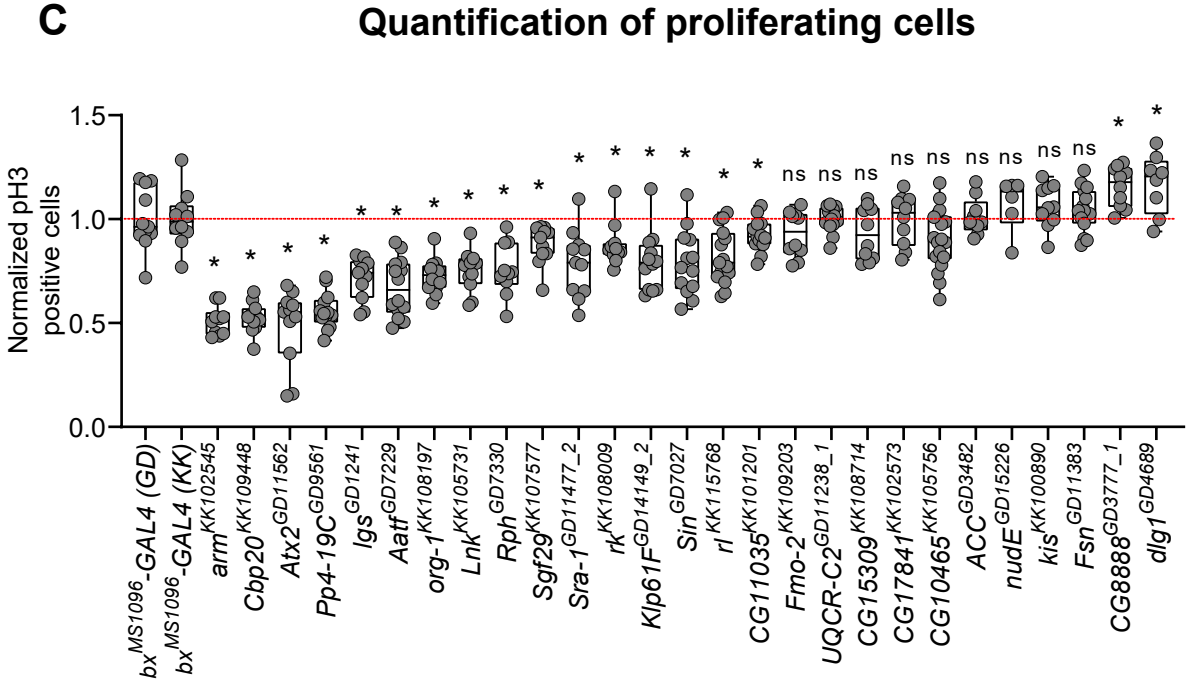
C
Quantification of proliferating cells
Normalized pH3 positive cells
bx^MS1096-GAL4 (GD)
bx^MS1096-GAL4 (KK)
arm^KK102545
Cbp20^KK109448
Atx2^GD11562
Pp4-19C^GD9561
lgs^GD1241
Aatf^GD7229
org-1^KK108197
Lnk^KK105731
Rph^GD7330
Sgf29^KK107577
Sra-1^GD11477_2
rk^KK108009
Klp61F^GD14149_2
Sin^GD7027
rl^KK115768
CG11035^KK101201
Fmo-2^KK109203
UQCR-C2^GD11238_1
CG15309^KK108714
CG17841^KK102573
CG10465^KK105756
ACC^GD3482
nudE^GD15226
kis^KK100890
Fsn^GD11383
CG8888^GD3777_1
dlg1^GD4689

Figure 7

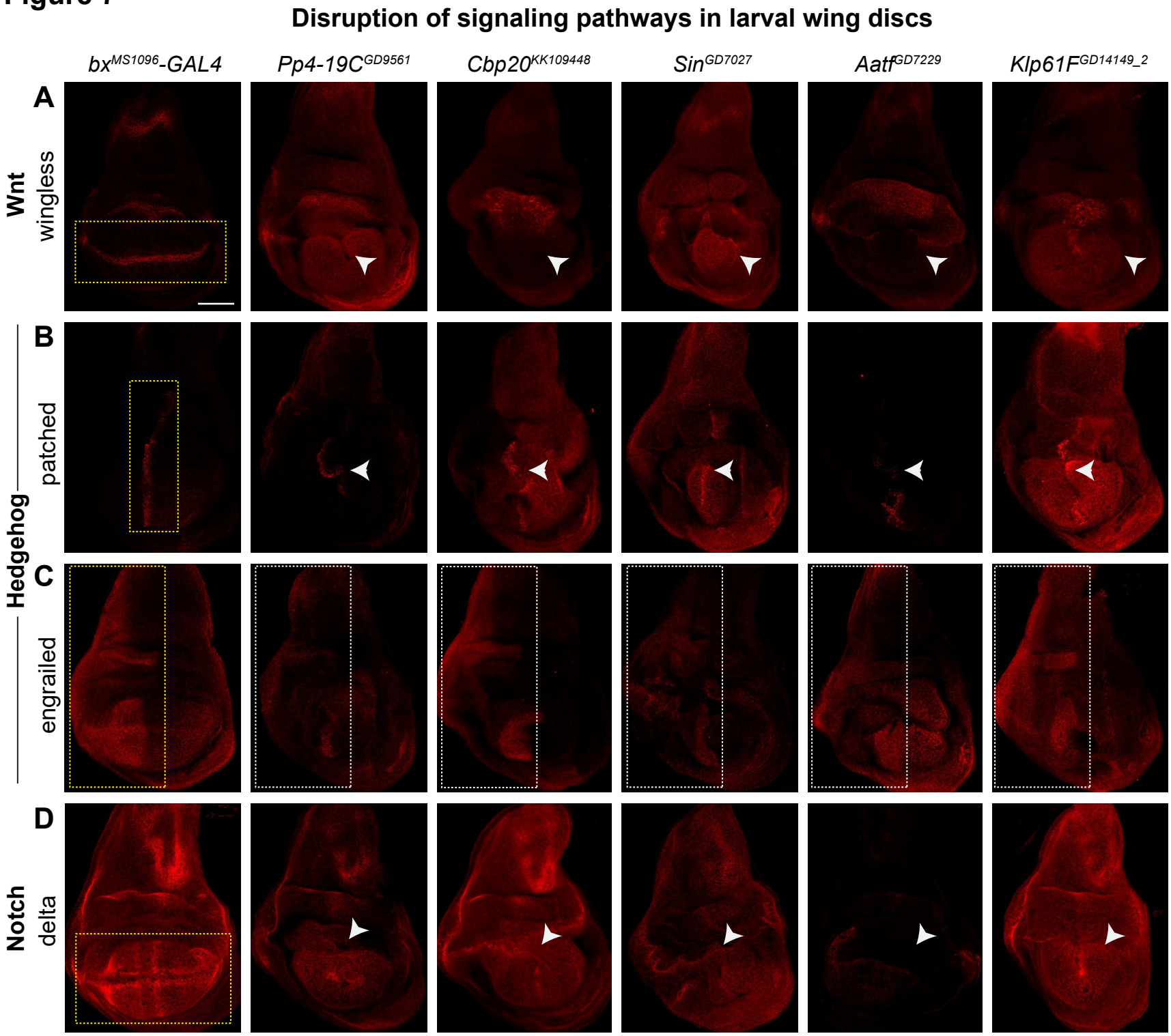
Disruption of signaling pathways in larval wing discs
bx^MS1096-GAL4
Pp4-19C^GD9561
Cbp20^KK109448
Sin^GD7027
Aatf^GD7229
Klp61F^GD14149_2
A
Wnt
wingless
B
Hedgehog
patched
C
engrailed
D
Notch
delta

Figure 8

A Human CNV genes interact with Notch signaling pathway genes in multiple tissues

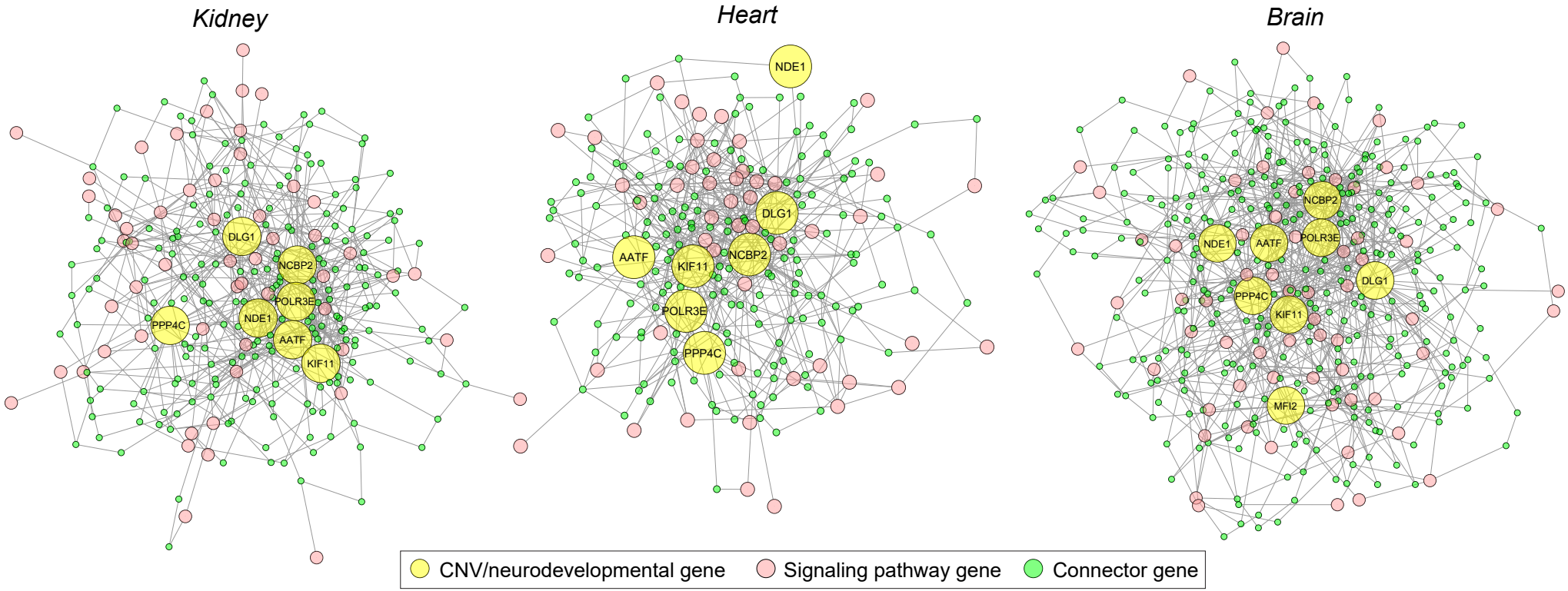

B Average connectivity of CNV genes to genes in signaling pathways

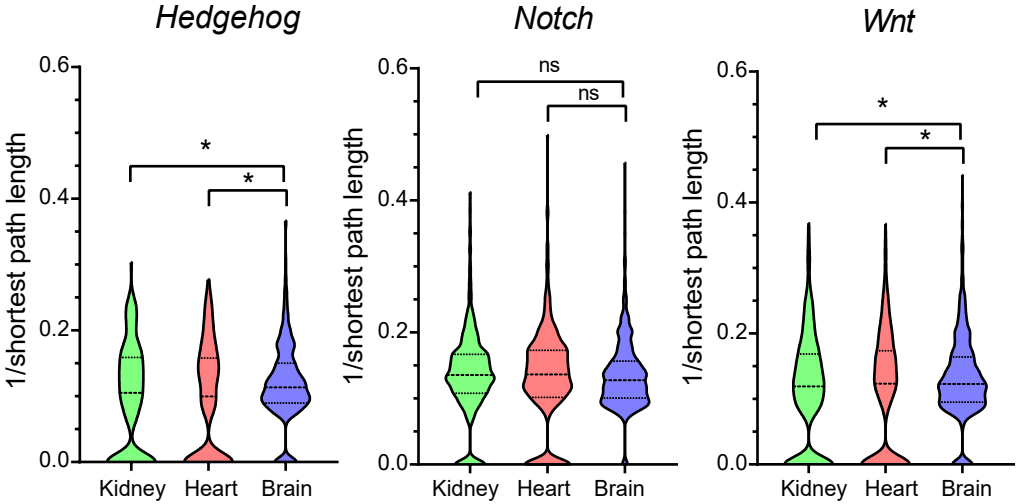

C GO term enrichment for connector genes in tissue-specific networks

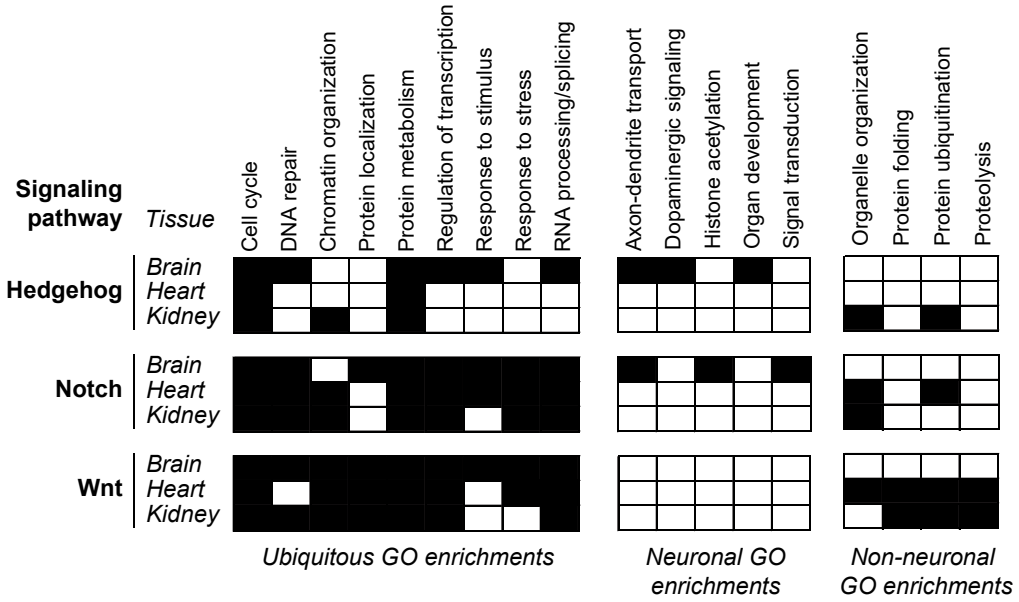

Figure 9

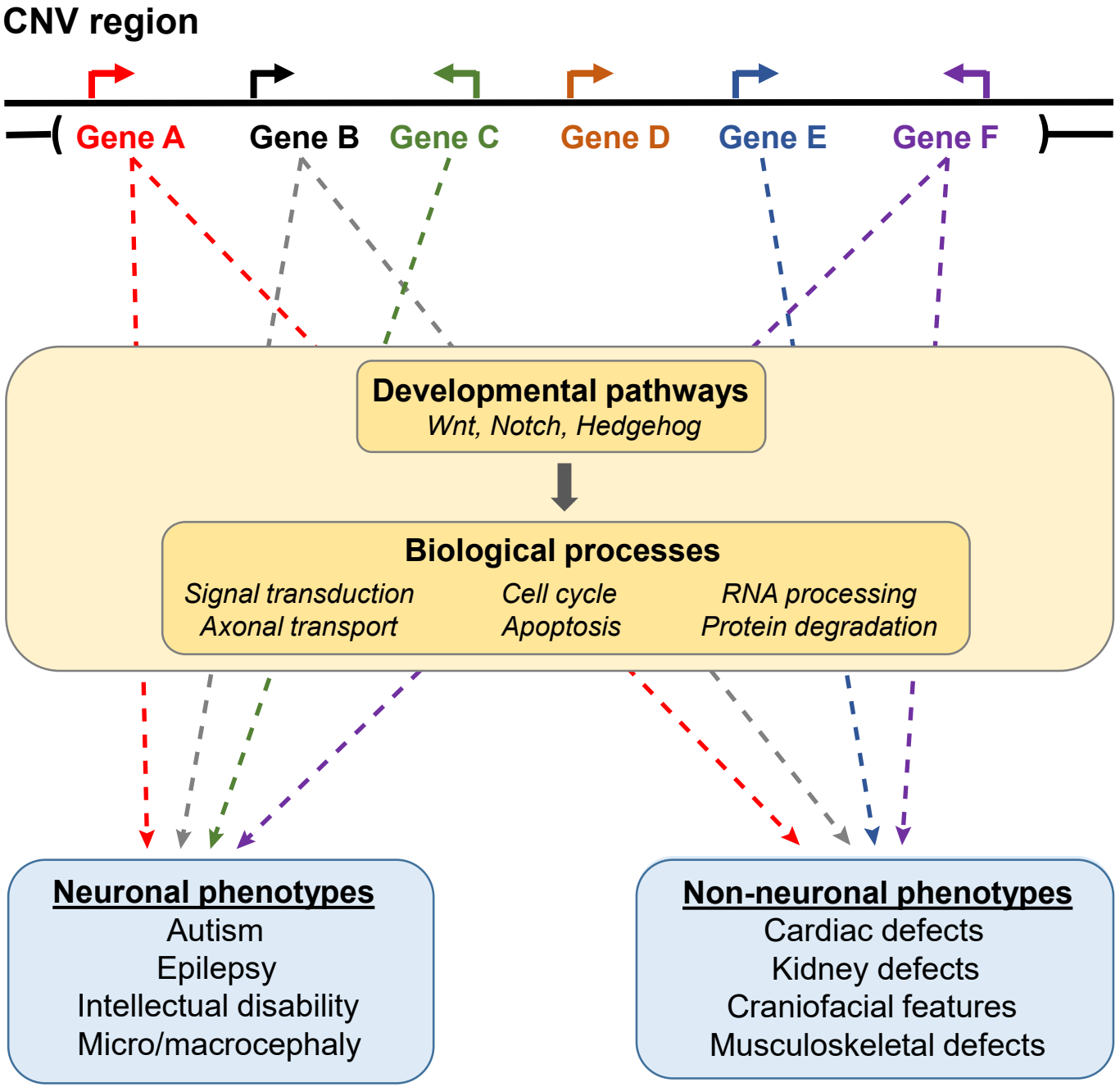
CNV region
Gene A
Gene B
Gene C
Gene D
Gene E
Gene F
Developmental pathways
Wnt, Notch, Hedgehog
Biological processes
Signal transduction
Axonal transport
Cell cycle
Apoptosis
RNA processing
Protein degradation
Neuronal phenotypes
Autism
Epilepsy
Intellectual disability
Micro/macrocephaly
Non-neuronal phenotypes
Cardiac defects
Kidney defects
Craniofacial features
Musculoskeletal defects

Supp. Figure 1

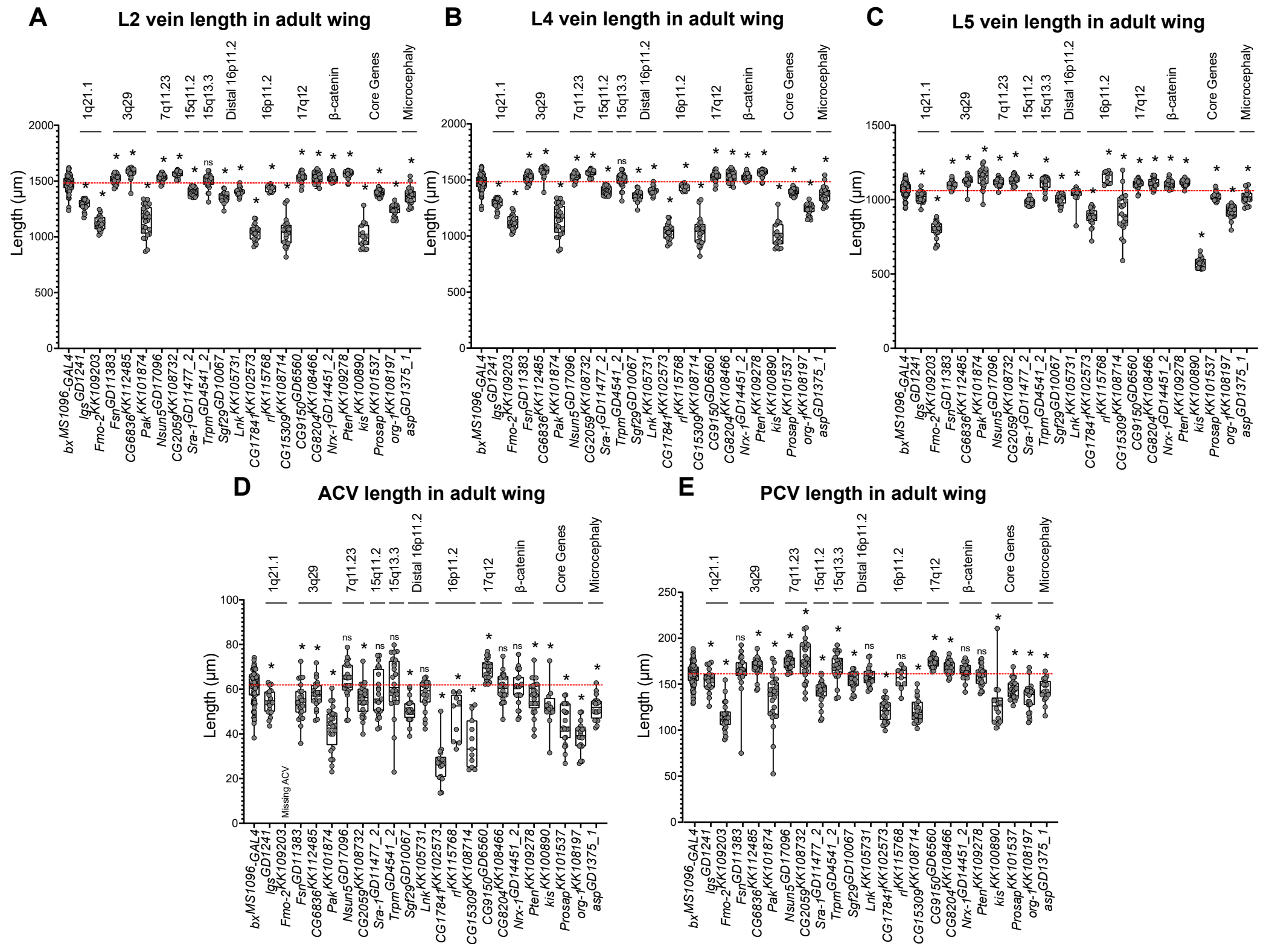

Supp. Figure 2

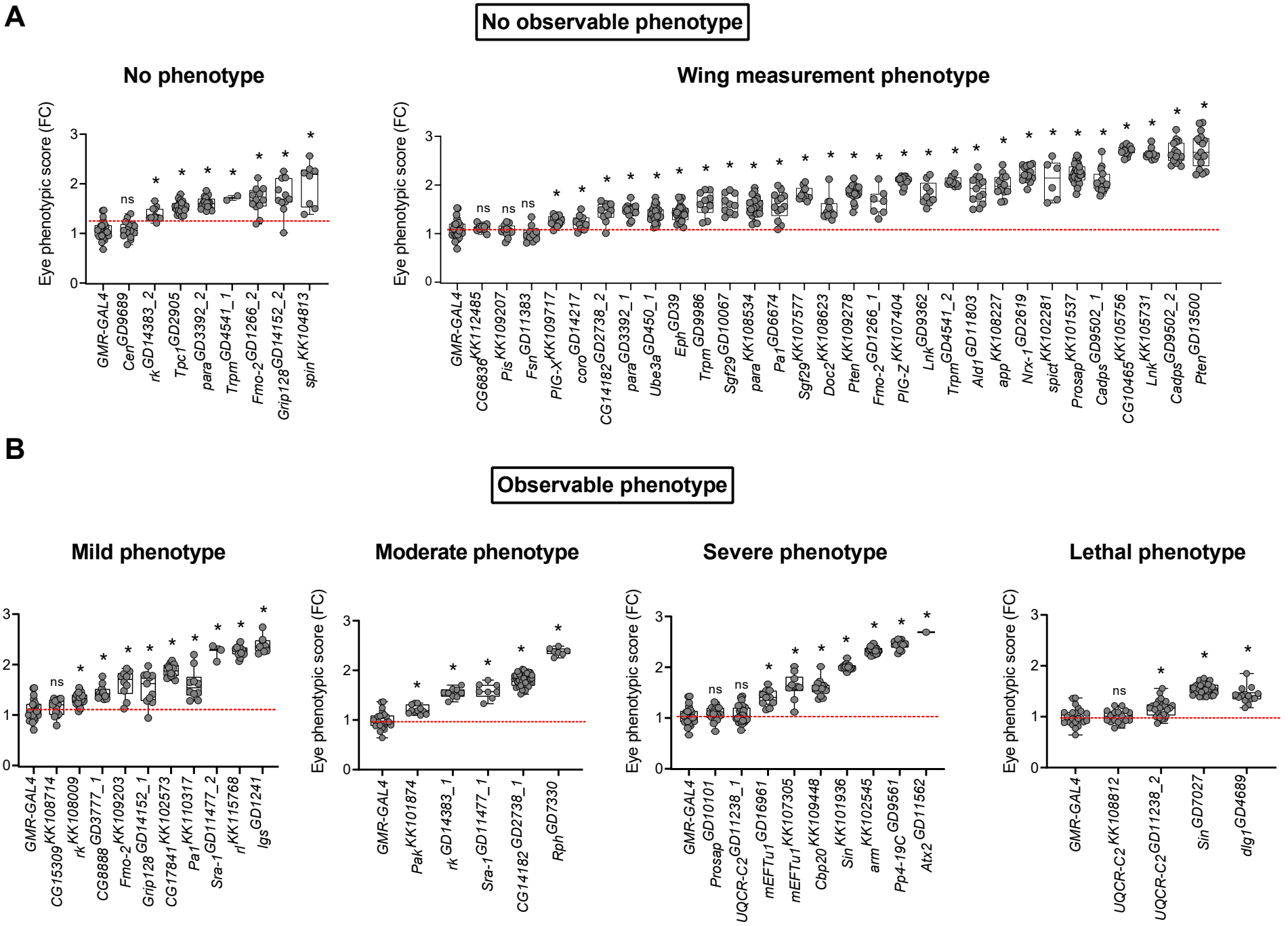

Supp. Figure 3

A Larval *Drosophila* expression

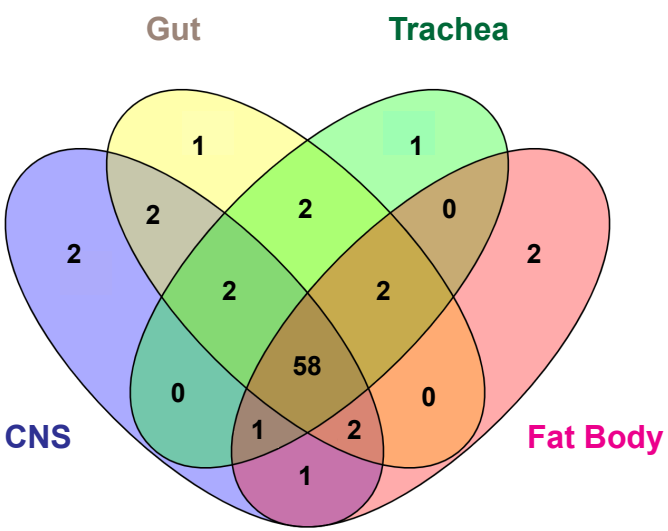

B Adult *Drosophila* expression

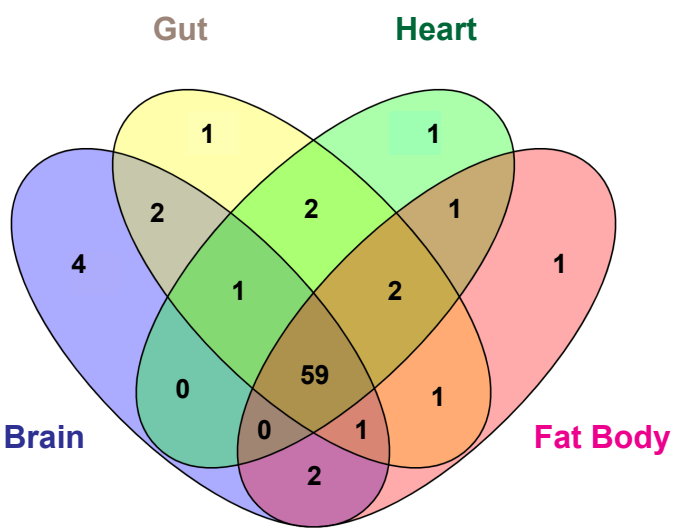

Supp. Figure 4

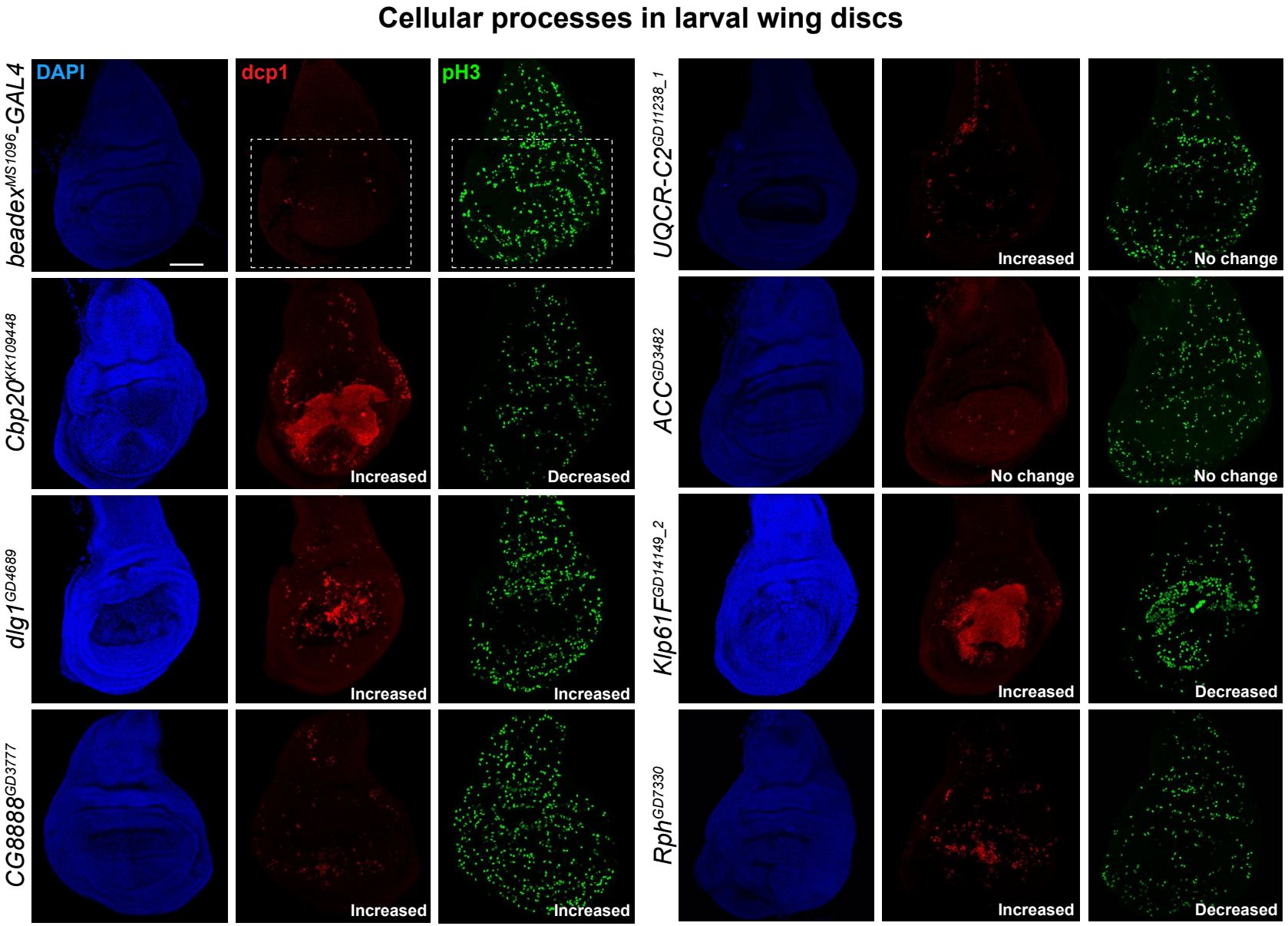

Supp. Figure 5

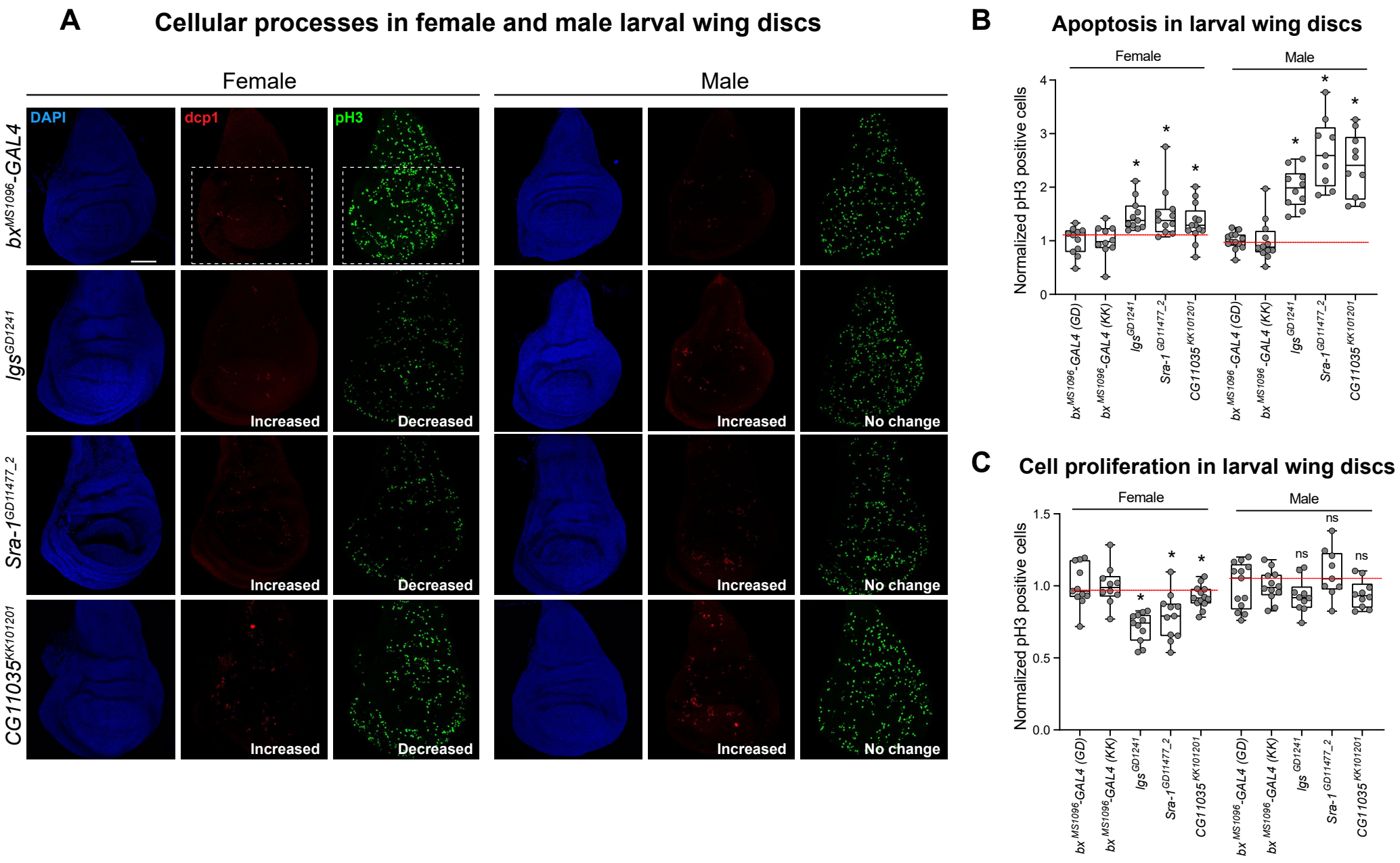

Supp. Figure 6

Disruption of signaling pathways in larval wing discs

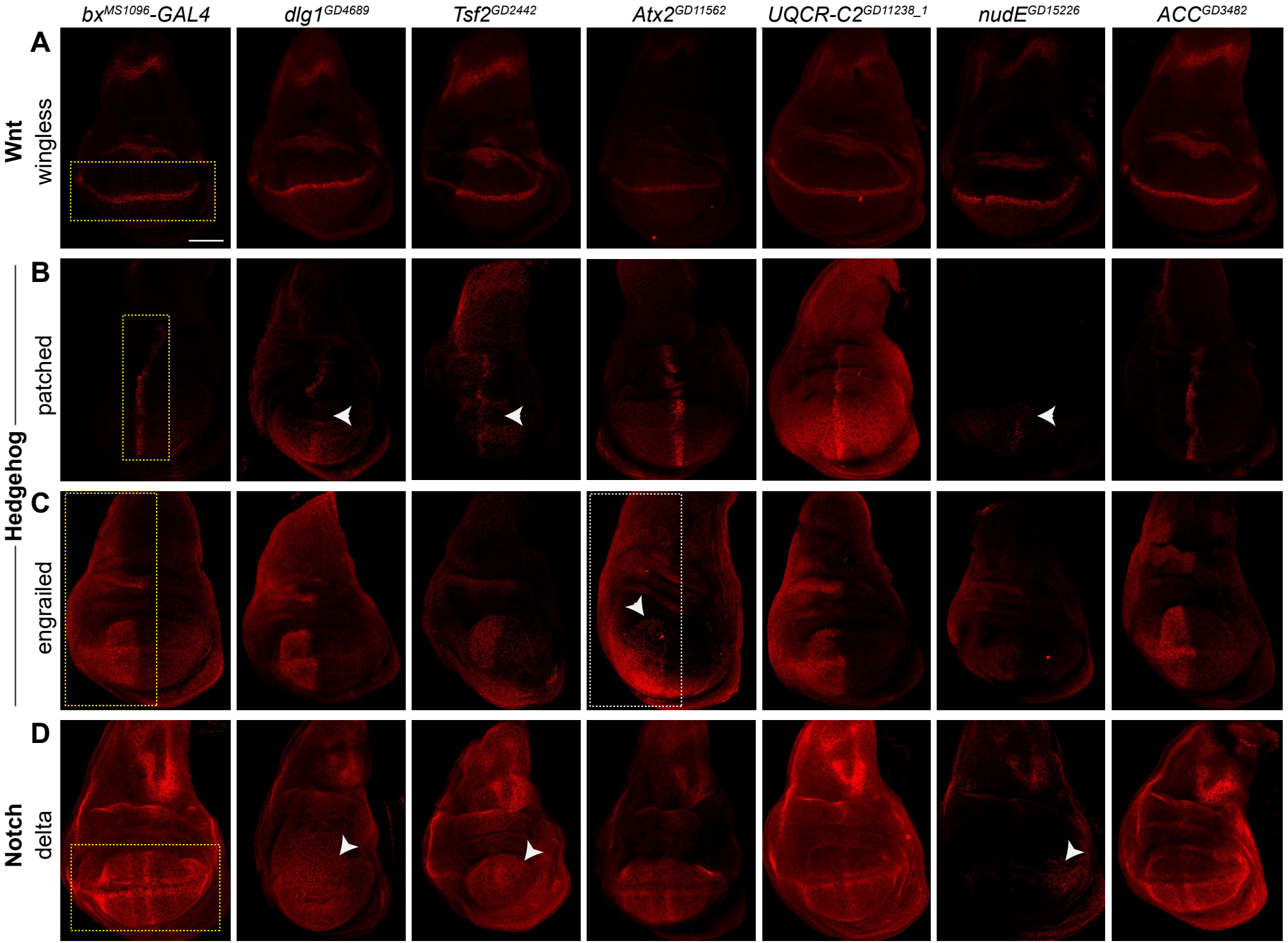

Supp. Figure 7